Atmospheric
Measurement
Techniques

A measurement system for CO₂ and CH₄ emissions quantification of industrial sites using a new in situ concentration sensor operated on board uncrewed aircraft vehicles

Jean-Louis Bonne[1], **Ludovic Donnat**[2], **Grégory Albora**[1], **Jérémie Burgalat**[1], **Nicolas Chauvin**[1], **Delphine Combaz**[1],
Julien Cousin[1], **Thomas Decarpenterie**[1], **Olivier Duclaux**[2], **Nicolas Dumelié**[1], **Nicolas Galas**[2], **Catherine Juery**[2],
Florian Parent[1], **Florent Pineau**[2], **Abel Maunoury**[2], **Olivier Ventre**[2], **Marie-France Bénassy**[2], and **Lilian Joly**[1]

[1]GSMA UMR 7331, Université de Reims Champagne-Ardenne, CNRS, Reims, 51100, France
[2]Air Quality Laboratory, TotalEnergies R&D, Solaize, 69360, France

Correspondence: Jean-Louis Bonne (jean-louis.bonne@univ-reims.fr) and Lilian Joly (lilian.joly@univ-reims.fr)

Abstract. We developed and tested a complete measurement system to quantify CO₂ and CH₄ emissions at the scale of an industrial site based on the innovative sensor Airborne Ultralight Spectrometer for Environmental Application (AUSEA), operated on board uncrewed aircraft vehicles (UAVs). The AUSEA sensor is a new light-weight (1.4 kg) open-path laser absorption spectrometer simultaneously recording in situ CO₂ and CH₄ concentrations at high frequency (24 Hz in this study) with precisions of 10 ppb for CH₄ and 1 ppm for CO₂ (when averaged at 1 Hz). It is suitable for industrial operation at a short distance from the sources (sensitivity up to 1000 ppm for CO₂ and 200 ppm for CH₄). Greenhouse gas concentrations monitored by this sensor throughout a plume cross section downwind of a source drive a simple mass balance model to quantify emissions from this source.

This study presents applications of this method to different pragmatic cases representative of real-world conditions for oil and gas facilities. Two offshore oil and gas platforms were monitored for which our emissions estimates were coherent with mass balance and combustion calculations from the platforms. Our method has also been compared to various measurement systems (gas lidar, multispectral camera, infrared camera including concentrations and emissions quantification system, acoustic sensors, ground mobile and fixed cavity ring-down spectrometers) during controlled-release experiments conducted on the TotalEnergies Anomaly Detection Initiatives (TADI) test platform at Lacq, France. It proved suitable to detect leaks with emission fluxes down to 0.01 g s⁻¹, with 24 % of estimated CH₄ fluxes within the −20 % to +20 % error range, 80 % of quantifications within the −50 % to +100 % error range and all of our results within the −69 % to +150 % error range. Such precision levels are better ranked than current top-down alternative techniques to quantify CH₄ at comparable spatial scales.

This method has the potential to be operationally deployed on numerous sites and on a regular basis to evaluate the space- and time-dependent greenhouse gas emissions of oil and gas facilities.

1 Introduction

After CO₂, methane is currently the second-most-important anthropogenic greenhouse gas in terms of climate forcing (Etminan et al., 2016), with effective radiative effects between 1750 and 2019 of 0.54 ± 0.11 W m⁻² for CH₄ compared to 2.1 ± 0.26 W m⁻² for CO₂ (Forster et al., 2021). Methane was brought to the center of the political debate, with new pledges of parties to consider further actions to reduce non-carbon dioxide greenhouse gas emissions by 2030 (Glasgow Climate Pact; UNFCCC, 2021). Due to its short lifetime of 11.8 ± 1.8 years in the atmosphere (Forster et al., 2021), reducing CH₄ emissions would be effective in terms of climate mitigation on short timescales (Shindell et al., 2012): fossil CH₄ emissions have a global warming potential of 82.5 ± 25.8 over 20 years but of 29.8 ± 11 over 100 years, in comparison with CO₂, with a reference global warming

potential of 1.0 (Forster et al., 2021). Climate mitigation actions including fast and deep methane emissions reduction would limit climate overshoot linked with a concomitant decrease in climate cooling aerosols emissions (Masson-Delmotte et al., 2018). Large uncertainties exist in the variations of many methane anthropogenic and natural sources and sinks (Saunois et al., 2020). A recent study indicates that anthropogenic fossil CH_4 emissions may have been underestimated by about 25 % to 40 %, representing about 38 to 58 Tg CH_4 yr^{-1} (Hmiel et al., 2020).

According to inventories, the oil and gas (O&G) sector is responsible for 22 % of the global anthropogenic methane emissions (Saunois et al., 2020). O&G facilities can emit methane from multiple sources (high-elevation stacks and flares, common or local vents, fugitive sources) of different nature (process venting; incomplete combustion during flaring, power generation, heating, etc; unintentional leaks) (Oil and Gas Methane Partnership (OGMP) 2.0 Framework, 2022). O&G operators currently report their methane emissions to their stakeholders, based on calculations using bottom-up approaches (Ng et al., 2017), including flow meters inside the plant, emission factors, modeling and Leak Detection And Repair (LDAR) campaigns. Such methods hardly capture temporal variations of emissions or unexpected operations and are furthermore poorly adapted to fugitive or diffuse emissions. This is an important issue as recent estimates suggested that fugitive emissions represent a significant part of emissions from O&G activities and could be strongly underestimated (Alvarez et al., 2018). Fugitive emissions might have been increasing in recent years, which would partly explain the global methane atmospheric concentration increase observed since the mid-2000s (Worden et al., 2017).

Top-down approaches, based on atmospheric measurements, can complement and validate bottom-up flux estimates. Developing technics able to be implemented on industrial facilities are necessary, either for fast leak detection or for quantification of long-term greenhouse gas emissions. They should be validated via controlled-release experiments, which can be organized within intercomparison campaigns (Ravikumar et al., 2019; Feitz et al., 2018). Such controlled-release campaigns are for example organized yearly on the TotalEnergies Anomaly Detection Initiatives (TADI) infrastructure in Lacq, southwestern France (43.41° N, −0.64° W), an industrial area dedicated to the simulation of a real-size oil and gas facility, used by international groups to validate their emission detection or quantification techniques (Kumar et al., 2021; Druart et al., 2021).

At the facility scale, different top-down emissions quantification approaches already exist, relying on both in situ and remote sensing measurements. Some methods, well adapted to emissions quantification on flat terrains such as landfills, like eddy covariance, stationary mass balance methods and radial plume mapping (Mønster et al., 2019), cannot be adapted to all industrial contexts with complex topography

and high-elevation sources. In situ atmospheric concentration measurements at the surface can be obtained from analyzers at a fixed position or on mobile platforms such as in cars for onshore facilities (Brantley et al., 2014; Ars et al., 2017; Feitz et al., 2018; Yacovitch et al., 2020; Kumar et al., 2021) or on board ships for offshore facilities (Nara et al., 2014; Riddick et al., 2019; Yacovitch et al., 2020). Other methods based on airborne observations have the advantage of measuring concentrations directly inside the plume. Observations can be performed from aircraft for onshore (Terry et al., 2017; Hirst et al., 2013; Lee et al., 2018; Conley et al., 2016, 2017; Gorchov Negron et al., 2020) or offshore facilities at the scale of an individual platform or of a whole basin (Gorchov Negron et al., 2020; France et al., 2021; Fiehn et al., 2020) but with a high logistical and financial cost and at a long distance from sources. The choice of the type of mobile platform is a key parameter, as it will determine the speed at which measurements are performed, and difficulties may appear with low-speed platforms, for example, when the plume is changing direction over the monitoring period or if areas cannot be accessed (limitations by the road infrastructure for cars, minimum distance to the facilities of minimum flight elevations for aircraft measurements, observations restricted to low elevations for cars or ships). UAV-based observations are adapted to the scale of industrial facilities, including offshore, and might answer these challenges. UAVs may indeed operate at lower costs than aircraft. They provide high speed and reactivity, allowing them to fly at shorter distances from the sources compared to aircraft or boats. This facilitates validation by controlled-release experiments and induces a gain in sensitivity as dilution of effluents will be lower at short distance from the source. The possibility of flying inside industrial sites also permits the emission sources to be better localized.

For quantifying emission fluxes based on airborne concentration measurements, two main approaches are generally adopted. The first approach is based on the inversion of modeled Gaussian plumes (Hirst et al., 2013; Lee et al., 2018; Shah et al., 2020). The Gaussian-based inversion methods are commonly applied to ground mobile observations (Brantley et al., 2014; Kumar et al., 2021) or to the localization of multiple unknown sources (Hirst et al., 2013; Huang et al., 2015; Brereton et al., 2018). Recent UAV-based experiments have relied on a near-Gaussian inversion approach but have so far suffered from important uncertainties (Shah et al., 2020), which might be improved in future (adapted measurement protocol or quantification model). The second approach is a mass balance method consisting in comparing the fluxes of gas entering and exiting a box around a source. It does not rely on any atmospheric model but is a direct quantification of the flux based on its integration through a surface. The main difficulties associated with this method are the ability to measure the concentrations throughout the whole plume and having precise knowledge of the wind conditions. This type of approach was originally employed for DIAL (dif-

ferential absorption lidar) quantifications, providing state-of-the-art volatile organic compound (VOC) quantification in complex industrial plants (NF EN 17628, 2022), and was already applied to greenhouse gas emissions quantification at various scales from industrial sites to large cities based on UAV or aircraft observations (Mays et al., 2009; Karion et al., 2015; Nathan et al., 2015; Allen et al., 2019; Fiehn et al., 2020; Morales et al., 2022). Contrary to Gaussian-based inversion models, mass balance does not require the assumptions of constant and continuous emissions, creating a steady-state system with normally distributed pollutant concentrations over a flat and uniform terrain, which is often not applicable to onshore or offshore fields.

Identification and quantification of CO_2 and/or CH_4 sources via top-down UAV-based approaches atmospheric concentration measurements of these species with a very low response time and high frequencies are preferable to be able to detect small plumes with UAVs flying at elevated speeds. Required precisions and sensitivity ranges depend on the expected amplitude of the signal. For applications to oil and gas industries, a large range of measurable concentrations are required, as high concentrations above the background level are expected; therefore the precision might be low as long as there is a good signal-to-noise ratio. Accurate analyzers are not required but their linearity is important since relative concentrations compared to the background levels are used. Different types of methane sensors suitable for UAV sampling already exist. Metal oxide gas sensors (Neumann et al., 2013; Malaver et al., 2015; Liu et al., 2020; Rivera Martinez et al., 2021) or cryptophane-A-cladded Mach–Zehnder interferometers (Dullo et al., 2015) are compact and competitive in price but with a relatively high detection limit and low response time (17 ppm of CH_4, 10 s response time) (Dullo et al., 2015). Miniaturized laser-based sensors have also emerged in recent years (Berman et al., 2012; Khan et al., 2012; Golston et al., 2017, 2018; Nathan et al., 2015; Shah et al., 2020; Tuzson et al., 2020) but do not necessarily have a large sensitivity range, a low response time and a light weight below 2 kg and generally measure only one species. Tunable diode laser absorption spectroscopy (TDLAS) allows a high selectivity and sensitivity in the gas detection and is considered the most advantageous technique for measuring atmospheric gas concentrations (Durry and Megie, 1999). Many applications are already based on this technique, not only UAV applications, among which are cavity ring-down spectroscopy (CRDS) (Crosson, 2008; Chen et al., 2010), cavity enhanced absorption spectroscopy (CEAS) (Romanini et al., 2006), integrated cavity output spectroscopy (ICOS) (O'Keefe, 1998; O'Keefe et al., 1999) and the most straightforward direct absorption spectroscopy (DAS) (Xia et al., 2017). Compared to closed-path DAS, open-cavity instruments are more sensitive to environmental perturbations, such as temperature and pressure variations or perturbations by solar radiations, but they have the advantage of a substantially enhanced response time to concentrations changes.

They also do not require pumps or cell temperature and pressure regulation systems, sparing substantial weight and energy. DAS is well adapted to in situ measurements and can be applied to sensors light enough to be embarked on UAVs, which led to the choice of technology adopted for the development of the sensor presented in this study.

In this study, we present a newly developed UAV-embarked CO_2 and CH_4 in situ analyzer and a methodology of emissions quantification adapted to the monitoring of O&G facilities. We present the characterization of this analyzer for the environmental conditions of its field applications. Our emissions quantification method was validated against CH_4 controlled releases in an intercomparison effort during the TADI campaigns of 2019 and 2021, together with other quantification methods using varied technologies: multispectral cameras, ground-based CRDSs (fix stations or mobile measurement in a car), wind and gas lidar, infrared cameras including concentrations and emissions quantification system, or tunable diode lidar. As a large part of TotalEnergies production activities are offshore-based, we present an application of our method to the quantification of emissions of two offshore gas production platforms in the North Sea.

2 CO_2, CH_4 and H_2O analyzers for UAV in situ observations

2.1   Technical description

A new sensor has been developed for in situ CO_2 and CH_4 observations able to operate on board UAVs (see Fig. 1): the Airborne Ultra-light Spectrometer for Environmental Application (AUSEA). It is based on the technical concept of the AMULSE instrument (Joly et al., 2016, 2020). As for the AMULSE instrument, the AUSEA instrument includes an open-path infrared laser absorption spectrometer using two DFB interband cascade laser diodes in the mid-infrared spectral region (NIR): near 4 μm with a direct path of 11 cm to measure CO_2 concentrations and near 3 μm in a homemade Herriott multipass cell of 3.5 m path length to measure CH_4 concentrations. The measurement frequency is of 24 Hz.

Compared to the AMULSE instrument, the AUSEA instrument has been adapted to reduce its weight; to adapt its sensitivity range to industrial applications (up to 1000 ppm in CO_2 and up to 200 ppm in CH_4); to limit the effect of vibrations, air turbulence and magnetic perturbations; and to implement air–ground communication for a real-time visualization of the concentrations by the operators. It has a power consumption of 8 to 15 W in most usual cases, depending on the external temperature (with maximal power consumption of 30 W during less than 1 s at start-up). It can be powered either with dedicated batteries for an average lifetime of 1.5 h or directly by the UAV. The instrument is also equipped with an iMet-4 from InterMet Systems (modified to fit in the instrument) to record air temperature (repeatability of

Figure 1. Picture of the AUSEA 112 analyzer mounted on a DJI M300.

0.2 °C, response time at 2 s for still air and < 1 s at 5 m s^{-1} and 1000 hPa), pressure (response time of 0.5 ms, 1.0 hPa uncertainty, 0.75 hPa reproducibility) and relative humidity (response time of 0.6 s at 25 °C or 5.2 s at 5°C and repeatability of 5 %) at 1 Hz frequency. Temperature, pressure and humidity values measured by the iMet-4 are used by the inversion process to account for their spectroscopic effects on the CO_2 and CH_4 absorption lines. The humidity value measurement by the iMet-4 can be employed to calculate the concentration in dry air, considering the dilution effect of the water vapor.

To monitor the position of the instrument, a lidar Lightware LW20/C measures the distance to the ground, and an Adafruit GPS records position and time. Position data obtained from the UAVs themselves have also been used for post-processing as they have a better precision than the integrated GPS sensor. Altogether, the weight of the AUSEA sensor has been optimized down to 1.4 kg, including all previously listed hardware. The results presented in this study are based on experiments performed with two AUSEA instruments (hereafter named AUSEA111 and AUSEA112), in order to verify the reproducibility of performances between several analyzers. Laboratory tests were performed to evaluate the precision and stability of the instruments in controlled environments. Field applications are also presented, using these instruments, and will also be analyzed in terms of instrumental performances (analyzing in-flight precision).

2.2 In-lab CO_2 and CH_4 analyzer characterization

In-lab characterization of the stability and linearity was performed independently on AUSEA111 and AUSEA112 instruments and repeated in different periods in 2021 and 2022. For these experiments, each AUSEA instrument was placed in a custom-made atmospheric chamber in which air is continuously mixed and homogenized (using fans) and temperature is regulated (at laboratory temperature).

2.2.1 Stability

The stability experiments consisted in measuring the same air sample within the closed atmospheric chamber by the AUSEA instrument over several hours. For AUSEA112, two experiments are analyzed (conducted on 19 April 2022 for a duration of 3 h and 2 min and of 1 h and 13 min), while four experiments are analyzed for AUSEA111 (two were conducted on 8 June 2022 for respective durations of 1 h 35 min and 15 h 12 min, and two were conducted on 23 March 2022 for respective durations of 50 min and 1 h 50 min). Allan deviations, calculated from those experiments for both analyzers, are presented in Fig. 2 and Table 1. The precision of our measurements can be derived from these experiments: for CH_4, precisions are below 20 ppb at 2 Hz, below 10 ppb at 1 Hz, below 1 ppb at 10 s and below 0.2 ppb at 1 min, and for CO_2, precisions are below 2 ppm at 2 Hz, below 1 ppm at 1 Hz, below 0.1 ppm at 10 s and 0.01 ppm at 1 min. We note a minimum of precision for the instrument AUSEA112 at 60 s with a stagnation of performances for longer averaging periods, contrary to the instrument AUSEA111 which has a better longer-term stability.

For comparison, precisions (1σ) of a commercial Picarro Inc. model G2401 analyzer are 0.05 ppm for CO_2 and 0.5 ppb for CH_4 at 5 s, but this type of analyzer has very different applications from our sensor (weight of 26.9 kg). Other laser-based UAV-embarked technologies have reached precisions at 1 Hz for CO_2 of 0.6 ppm (Berman et al., 2012) and for CH_4 of 1 ppb (Tuzson et al., 2020), 2 ppb (Berman et al., 2012; Shah et al., 2020), 5 ppb (Golston et al., 2017) or 100 ppb (Nathan et al., 2015) but with various weights, power consumption or response times.

2.2.2 Linearity

To evaluate linearity, air samples of varying concentrations were simultaneously measured by the AUSEA analyzer placed in the atmospheric chamber and by a reference instrument pumping air from the atmospheric chamber. Air with high CH_4 concentration was initially injected into the atmospheric chamber and progressively mixed with room air, thus spanning a continuous range of concentrations from the initial sample up to ambient air levels. Variations of CO_2 concentrations were simply generated by natural variations of the CO_2 values in the laboratory air. The reference instrument used was a cavity ring-down spectrometer (Picarro Inc. model G2401), hereafter referred as the Picarro, with an operating range certified by the manufacturer from 0 to 1000 ppm for CO_2 and from 0 to 20 ppm for CH_4. The Picarro has been validated through the ICOS Atmospheric Thematic Center protocol (Yver Kwok et al., 2015) and was calibrated using the standard procedure for ICOS atmospheric monitoring stations with four calibration standards of known CO_2 and CH_4 concentration ranging from 396.05 to 504.16 ppm for CO_2 and 1807.7 to 2346.5 ppb for CH_4
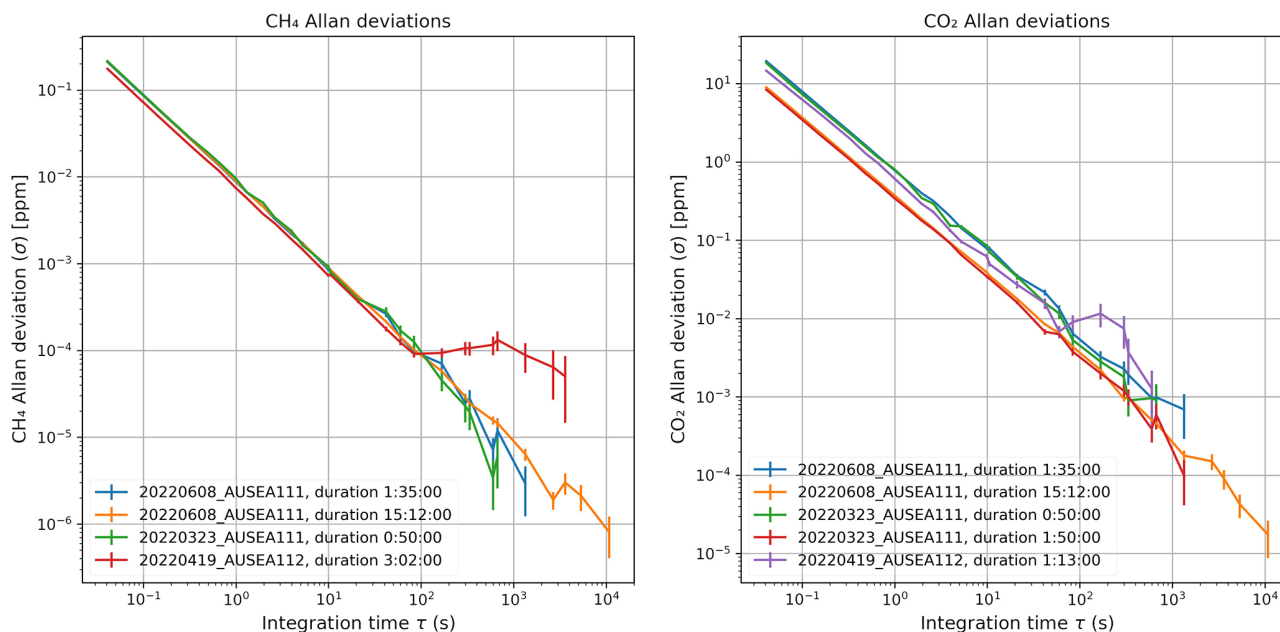
Figure 2. Allan deviations calculated for multiple stability experiments with analyzers AUSEA_111 and AUSEA_112.

Table 1. Precisions of the AUSEA111 and AUSEA112 analyzers at given frequencies (0.5, 1, 10, 60 s) derived from Allan deviations of stability experiments performed on different dates, expressed in parts per billion (ppb) for CH_4 and parts per million (ppm) for CO_2.

Instrument	Date (yyyy-mm-dd)	Duration	Species (unit)	$\sigma_{0.5\,s}$	$\sigma_{1\,s}$	$\sigma_{10\,s}$	$\sigma_{60\,s}$
AUSEA111	2022-06-08	1 h 35 min	CH_4 (ppb)	18	9	0.8	0.1
AUSEA111	2022-06-08	15 h 12 min		18	9	0.9	0.1
AUSEA111	2022-03-23	50 min		19	10	0.9	0.2
AUSEA112	2022-04-19	3 h 2 min		15	8	0.7	0.1
AUSEA111	2022-06-08	1 h 35 min	CO_2 (ppm)	1.6	0.8	0.1	0.01
AUSEA111	2022-06-08	15 h 12 min		0.8	0.4	0.04	0.01
AUSEA111	2022-03-23	50 min		1.5	0.8	0.1	0.01
AUSEA111	2022-03-23	1 h 50 min		0.7	0.3	0.03	0.01
AUSEA112	2022-04-19	1 h 13 min		1.3	0.6	0.06	0.01

(ICOS RI, 2020). AUSEA and Picarro analyzer data were compared at a Picarro temporal resolution of 5 s. Linearity experiments were conducted on 23 March 2022 and 8 June 2022 for AUSEA111 and on 15 April 2021 and 19 April 2022 for AUSEA 112. Linearity experiment covered CO_2 and CH_4 concentrations ranging from 429.0 to 861.4 ppm of CO_2 and from 2.1 to 20.00 ppm of CH_4 (within the reference instrument certified linearity domain).

The results of the linearity experiments are presented in Fig. 3 and Table 2. An excellent linearity was observed for both species for each experiment: linear regressions provide excellent coefficients of determination R^2 of 1.0 for CH_4 and CO_2, with p values (probability of obtaining tests results at least as extreme as the results actually observed) well below 10^{-5}, so with high statistical validity. Low residuals are observed for each linear regression (difference between mea-sured values and linear regressions), within 0.02 ppm of CH_4 and 1.5 ppm of CO_2 (Fig. 3), which corresponds to the precisions of the instruments, and do not reveal deviations from a linear distribution. We observed relatively low variations of the slopes and intercepts of the linear regressions between repeated experiments over the course of several months (Table 2) and therefore of the instrument response (slopes and intercepts variations respectively below 2.3 % and 0.16 ppm for CH_4 and 1.6 % and 7 ppm for CO_2).

The linearity of our AUSEA sensor was experimentally validated for CO_2 concentrations between 429.0 and 861.4 ppm and CH_4 concentrations between 2.1 and 20 ppm, against the guaranteed linearity domain of a reference instrument validated by top-of-the-art metrology standards (Yver Kwok et al., 2015). However, the sensitivity domain of our AUSEA sensor exceeds these limits: the chosen pathlength
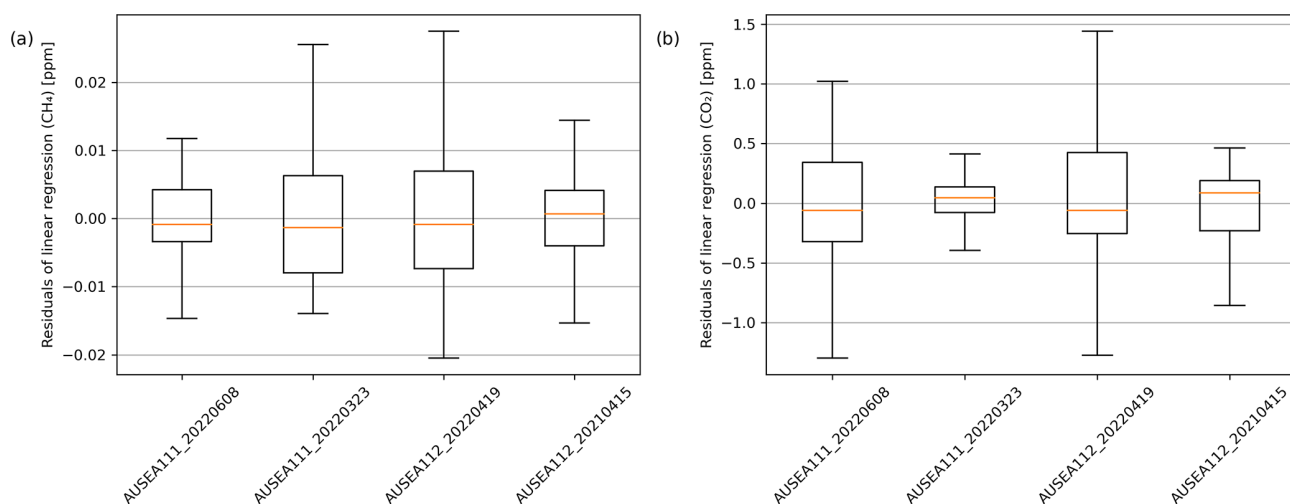
Figure 3. Box plots of the residuals of the linear regressions for each linearity experiment of the AUSEA sensor against a reference Picarro CRDS analyzer in a temperature-controlled environment at a 5 s temporal resolution. Box plots depict the first and last quartile (lower and upper borders of the boxes), median (orange line), and minima and maxima (lower and upper ticks, defined as the first and last quartile plus or minus 1.5 times the interquartile range), without outliers.

Table 2. Results of the linearity experiments for instruments AUSEA111 and AUSEA112 performed at different dates, for the CH_4 and CO_2 measurements: range of concentrations covered by the experiments (minimum and maximum values), slope and intercept of the linear regressions of the distributions (only values below 20.0 ppm for CH_4), and associated R^2 values and number of data points at a 5 s frequency resolution used for the linear regression.

Instrument	Date (yyyy-mm-dd)	Species	Minimum (ppm)	Maximum (ppm)	Slope	Intercept (ppm)	R^2	N
AUSEA112	2021-04-15	CH_4	2.1	20.0	1.009	+0.03	1.0	30 751
	2022-04-19		2.2	20.0	1.032	+0.163	1.0	17 169
AUSEA111	2022-03-23		3.2	20.0	1.008	−0.018	1.0	16 267
	2022-06-08		2.2	20.0	0.991	+0.024	1.0	5943
AUSEA112	2021-04-15	CO_2	429.0	509.9	1.007	+6.538	1.0	30 751
	2022-04-19		454.9	646.3	1.009	+6.2	1.0	17 169
AUSEA111	2022-03-23		465.3	657.8	1.011	+10.702	1.0	16 267
	2022-06-08		532.3	861.4	0.995	+17.7656	1.0	5943

for the CH_4 measurements has been determined to reach saturation around 200 ppm. Given the saturation of the CO_2 absorption spectrum, the maximum measurable concentration is limited to 1000 ppm (but this limit can be easily adapted by modifying the CO_2 laser-to-detector pathlength). Therefore, we believe the linearity domains also exceed the range of concentrations tested in the laboratory, up to 1000 ppm for CO_2 and above 100 ppm for CH_4. The lack of a reference instrument with a comparable certified linearity domain in our laboratory did not allow us to validate this limit so far. However, additional linearity experiments conducted with the same reference CRDS instrument, not presented here, for CH_4 concentrations up to 100 ppm also depicted an excellent linearity (also with R^2 of 1.0 and $p < 10^{-5}$ for 24 975 data points), therefore giving confidence in the linearity of our AUSEA sensors, even for concentrations out of the CRDS in-

strument manufacturer's certified linearity domain. This confidence is also motivated by the fact that the same type of CRDS analyzers was also employed for the quantification of industrial emissions of CH_4, with peaks up to approximately 90 ppm (Kumar et al., 2021; Jackson et al., 2014).

3   Source emissions quantification

A mass balance method has been developed to quantify source emissions from atmospheric concentration measurements. It relies on the airborne monitoring of atmospheric concentrations of the species of interest from UAV and of the wind speed and direction at the elevations of the UAV.

3.1 Monitoring method

3.1.1 Measurements on board uncrewed aircraft vehicles

The AUSEA instrument is embarked on a low-weight (below 8 kg payload) commercial multicopter. Several models of UAVs have been employed (DJI M200, DJI M210, DJI M300 and a non-commercial drone), able to fly under wind speeds of up to $12\,\mathrm{m\,s^{-1}}$, with autonomies of 20 to 45 min. The instrument was always integrated between both UAV landing gears, below the propellers' level (see Fig. 1). Concentration measurements are remotely monitored in real time by the operators on the ground (usually a pilot and a co-pilot), allowing the plume to be located and the trajectory of the UAV to be optimized to fit the flight plan requirements of the emissions quantification method.

3.1.2 Wind profile meteorological parameter measurements

Wind speed and direction profiles are recorded by a commercial ZX300 Doppler wind lidar (from ZX Lidars Inc.), equipped with an AIRMAR weather station at 2.5 m above ground level (or m a.g.l.). The lidar records wind speed and direction at 10 elevations between 11 and 300 m a.g.l., completed by wind measurements at the AIRMAR station, thus covering the range of altitudes of the UAV tracks. The AIRMAR station also records temperature, relative humidity and air pressure. Wind measurements have an approximate 15 to 20 s time resolution (all levels are monitored successively within about 1 to 2 s), with precisions of $0.1\,\mathrm{m\,s^{-1}}$ for the wind speed (WS) and of $0.5°$ for the wind direction (WD). The wind speed and direction are interpolated at the elevations of the UAV. For elevations below the first height of lidar measurements, a logarithmic interpolation with assumption of null wind speed at the ground level is used, following the shape of a neutral wind profile. For levels above the first lidar measurement height, the interpolation is linear.

3.1.3 UAV flight protocol

Our protocol for UAV-based atmospheric concentrations monitoring was designed for our quantification model. The UAV flight plan should meet the conditions described hereafter (see Fig. 4). Concentration measurements are performed downwind of the sources, within a vertical plane crossing the plume, later referred as the observational plane. The observational plane must be as close as possible to a plume cross-section and therefore orthogonal to the prevailing wind direction. Several horizontal transects covering the entire plume and part of the surrounding background are recorded within this plane, with elevations distributed from below (or closest to the ground possible) to above the plumes. A precise wind speed and direction monitoring covering the range of altitudes of the UAV must be conducted simultaneously.

3.2 Emissions quantification model

An emission quantification approach has been tested to take advantage of the UAV observations. It is based on a mass balance approach, as also applied in the literature for similar UAV-based flight scenarios (Yang et al., 2018; Andersen et al., 2021; Morales et al., 2022): the emission rate Q (in $\mathrm{g\,s^{-1}}$) is estimated from a flux through the observational plane crossing the plume of emissions. It assumes constant emissions during the monitoring period and no degradation of effluents through chemical reactions over the monitoring period, which is reasonable for CO$_2$ and CH$_4$. The frame reference (x, y, z) is defined by the observational plane (see Fig. 4), with x in the horizontal direction orthogonal to the plane, y in the horizontal direction along the plane and z in the vertical direction. Q is equal to the integral across the plane, of the wind speed component along x, $u_x(y, z)$ (in $\mathrm{m\,s^{-1}}$) multiplied by the differential of dry basis volume concentrations (in $\mathrm{g\,m^{-3}}$, calculated from wet basis concentrations and the humidity measured by the iMet-4 sensor) between the plume $c_p(y, z)$ and the background $c_{bg}(y, z)$:

$$Q = \iint_{y,z} u_x(y, z) \cdot [c_p(y, z) - c_{bg}(y, z)]\,\mathrm{d}y\mathrm{d}z. \tag{1}$$

Background concentrations are assumed spatially uniform, $c_{bg}(x, y, z) = c_{bg}$, and estimated from the concentrations measured outside the plume. Wind speed is assumed horizontally uniform: $u_x(y, z) = u_x(z)$. As the wind direction might fluctuate over the complete monitoring period, we consider the average wind over the duration of each transect. Noting the angle $\alpha(z)$, often non-neglectable in practice, between the horizontal wind direction and the x axis, the component $u_x(z)$ of the wind speed can be expressed as a function of the total wind speed $U(z)$, as follows: $u_x(z) = \cos(\alpha(z)) \cdot U(z)$. Altogether, Eq. (1) becomes

$$Q = \int_z U(z) \cdot \cos(\alpha(z)) \cdot \left[\int_y (c_p(y, z) - c_{bg})\,\mathrm{d}y \right] \mathrm{d}z. \tag{2}$$

For the computation based on observation data, we first calculate the values of $q(z) = U(z) \cdot \cos(\alpha(z)) \cdot \left[\int_y (c_p(y, z) - c_{bg})\,\mathrm{d}y \right]$, the horizontal flux component (in $\mathrm{g\,s^{-1}\,m^{-1}}$) at each transect level z. The high horizontal resolution of the measurements allows a simple linear integration to be used to compute the horizontal integration. The integral of all $q(z)$ values along z is calculated from interpolated values of $q(z)$ profile, assuming neglectable vertical variations of the plume compared to the vertical gap between successive transects. Linear vertical interpolations are used between the values of $q(z)$ at each horizontal transect elevation z. If values
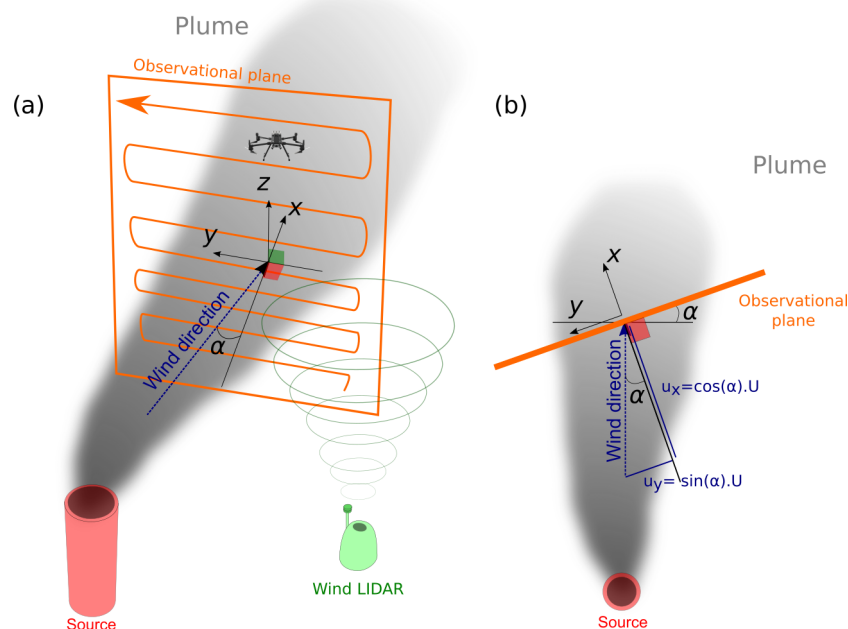
Figure 4. Schematic representation of the observation protocol: general 3D view **(a)** and top view **(b)**. The source (in red) emits a plume (grey shade). The UAV monitors the concentrations along a flight path (orange arrow), constituted of multiple horizontal transects, within a vertical observational plane, represented by the orange quadrangle in **(a)** and the orange line in **(b)**. The angle between the x axis and the horizontal wind direction is noted α. A wind lidar (green) measures the wind direction and speed at several elevations.

of $q(z)$ do not reach zero at the lowest or highest horizontal transect elevations, an extrapolation is performed using a logarithmic function, assuming that $q(z)$ must be equal to zero at the ground. This method can be applied in a wide range of meteorological conditions (limited by UAV maximum wind speeds limits) but is poorly adapted to low wind speeds and unstable wind directions, where measurement uncertainty can strongly rise (Yang et al., 2018; Morales et al., 2022).

3.3 Validation of emissions quantification method

3.3.1 Field validation protocol

Two validation campaigns were conducted from 1 to 10 October 2019 and from 7 to 10 September 2021 on the TotalEnergies Anomaly Detection Initiatives (TADI) platform in Lacq, in southwestern France ($43.41°$ N, $-0.64°$ W). The TADI platform, already described in the literature (Kumar et al., 2021, 2022), is an approximately $2000\,m^2$ rectangular area that is almost flat (Fig. 5), surrounded by agricultural land and rural settlements and with important chemical and industrial plants to the east of the platform. Multiple obstacles for dispersion are created by tents where other instruments are located, decommissioned oil and gas equipment and other small infrastructures. A road surrounding the north and east borders of the site cannot be flown over, limiting the area of UAV operations.

Several emission sources were spread over the platform, within a $40\,m \times 60\,m$ rectangular area classified as the "ATEX zone" (Fig. 5), out of reach for all participants due to security reasons. Sources were elevated between 0.1 and 6.5 m.a.g.l, originating from a variety of equipment (valve, connector, flange, drilled plug, tank, manhole, corrosion, flare pipe – no combustion, etc.). Either CO_2 or CH_4 or a combination of both species were emitted but also a mixture including a proportion of C_2H_6 or C_3H_8 to test if the method is able to differentiate these species from CH_4. Only CH_4 emissions quantification results are presented in this study (the low number of CO_2 releases does not allow statistical analysis of our CO_2 quantifications). Release scenarios had durations from 10 to 73 min (with two short leaks of 15 s and 2.5 min which were not monitored with our method), with pauses of approximately 5 min between two releases. Mass flow controllers were used to regulate and monitor the controlled CH_4 flow rates, with a large range of values from 0.01 to $150\,g\,s^{-1}$. This variety of emission sources, duration and amplitude is representative of the diversity of emission scenarios expected on industrial facilities. Information about the leaks (locations, species and fluxes) of each experiment can either be communicated (open trials) or withheld (blind tests) from the measurement teams. Results from both open trials and blind tests are presented.

For our UAV-based emission quantification method, one team was operating a DJI M200 in 2019, while two teams

Figure 5. Aerial view of the TADI platform with location of the emission sources (yellow crosses) and the explosive atmosphere area (ATEX zone, depicted as an orange square). Map data: Google, © 2022 Maxar Technologies.

were operating either a DJI M300 or a DJI M210 and a non-commercial UAV in 2021. CO$_2$ and CH$_4$ concentrations were measured on board these UAVs with an AUSEA analyzer (either AUSEA 111 or AUSEA112).

In 2021, all drones were equipped with RTK GPS positioning systems, which was not the case in 2019. Flight durations were from 10 to 20 min. Concentration measurements were performed within a vertical plane distant from the sources from approximately 20 to 80 m. As the sources were at low elevation (below 6.5 m), the plumes were monitored with a varying number of 5 to 15 low elevation horizontal transects distributed between 1 and 12 m a.g.l. in 2019 and up to 35 m.a.g.l in 2021. Wind speeds and directions were measured at 10 elevations between 11 and 300 m a.g.l. with the ZX300 wind lidar (equipped with the AIRMAR station at 2.5 m a.g.l.).

3.3.2 Results of validation experiments

An example of concentration measurements obtained during the TADI 2021 is presented in Fig. 6. Spikes of CH$_4$ concentrations up to 15 ppm linked to the emission plume can be observed well above the background level (around 2.1 ppm for this flight). The vertical distribution of the concentration measurement shows the highest spikes along a transect around 7 m a.g.l.

Figure 7 presents the horizontal components of the flux $q(z)$ at each horizontal transect elevation and the vertical interpolation of these values used for the computation of the vertical integration. The vertical profile of $q(z)$ shows a peak around 7 m elevation. Null values of $q(z)$ were correctly measured around 18 m elevation, describing the top of the plume. Low values of $q(z)$ were obtained at the lowest horizontal transect, but the bottom value did not reach zero (the lowest horizontal level is determined for safety reasons of UAV operation). Therefore, a logarithmic interpolation was performed to interpolate the values of $q(z)$ below the lowest transect, considering zero flux at the ground level. CH$_4$ emissions quantifications of the two TADI campaigns are analyzed hereafter and compared to the reference real fluxes derived from mass flow meters at the source. The emissions averaged quantifications for each controlled-release experiment are presented in Fig. 8, and the values are given in Tables S1 and S2 in the Supplement (with additional details for each flight). Statistical analyses of the results are presented in Tables 3 and 4.

During the two TADI campaigns, UAV measurements were conducted during 34 out of 41 controlled releases (among which 15 were blind tests) in 2019 and during 20 out of 24 controlled releases (all blind tests) in 2021. Emission quantifications could be successfully calculated with our method for respectively 26 and 18 controlled-release experiments in 2019 and 2021. Some release experiments could
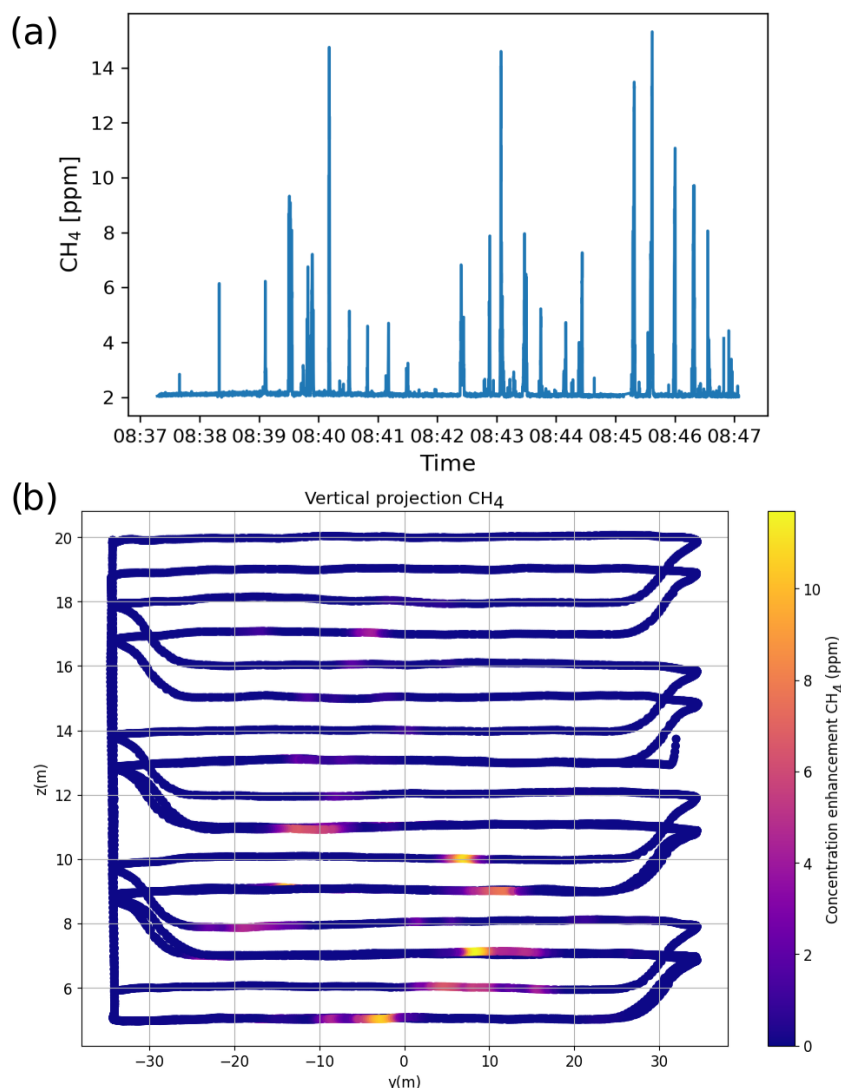
Figure 6. Measured CH_4 concentrations (ppm) during a flight of the TADI 2021 campaign corresponding to the monitoring of the 2021W36/10-22 controlled-release experiment performed on 10 September 2021: **(a)** time series and **(b)** distribution along the y horizontal axis (in m) and the vertical axis (altitudes in m a.g.l.) of the CH_4 concentrations above the background level.

not be quantified due to unavailability of the instruments, UAVs or pilots, and some of the quantification flights were discarded as the flight paths did not match our standards (e.g. did not cover the complete horizontal or vertical plume section, or technical issues were noticed with some of the sensors). Some of the controlled releases could be monitored by several independent flights (3 by 4 flights, 4 by 3 flights, 19 by 2 flights) and the rest (19 releases) could only be monitored once.

Figure 8 and Tables S1 and S2 present the averaged quantifications of all controlled-release experiments compared to the real fluxes. The relative errors of the average of quantifications are also given in Tables S1 and S2. The relative errors of our quantification compared to the true values show that out of 45 quantified controlled releases, 24 % relative errors

were between −20 % and +20 % compared to the true values (11 out of 45 controlled releases; see Fig. 8), and 80 % of our quantifications had relative errors between −50 % and +100 % (36 out 45 controlled releases; see Fig. 8). Among all 45 quantifications of the TADI campaigns, the relative errors of all quantifications span −69 % to +149 % (Table 3), which is representative of the global precision of the quantification method. In terms of total emitted mass during all of the TADI campaigns, the relative error of our quantifications is −41 %, taking into account all the quantified releases, but this total is strongly biased by the highest release 2019W41-SAT at $150 \, g \, s^{-1}$ during 1 h 13 min. By discarding values associated with this release, the relative error of our quantifications is −12 % only.
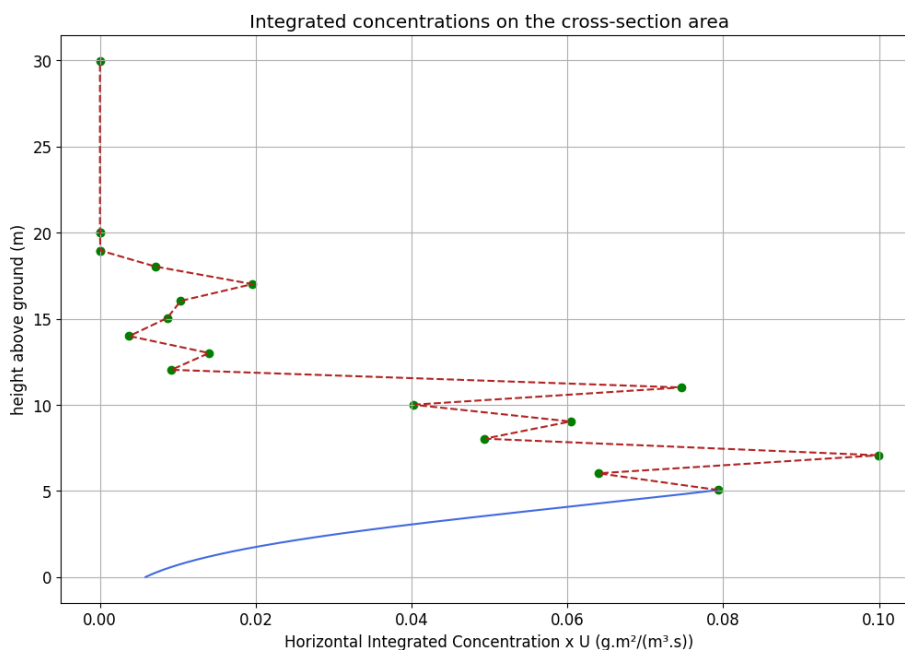
Figure 7. Vertical distribution of the horizontal flux components $q(z)$ (in $g\,s^{-1}\,m^{-1}$) at each transect level z (green dots), along with the interpolation used for the vertical integration (dotted red curves for linear interpolation and plain-blue curve for logarithmic interpolation), for the same flight as Fig. 6.
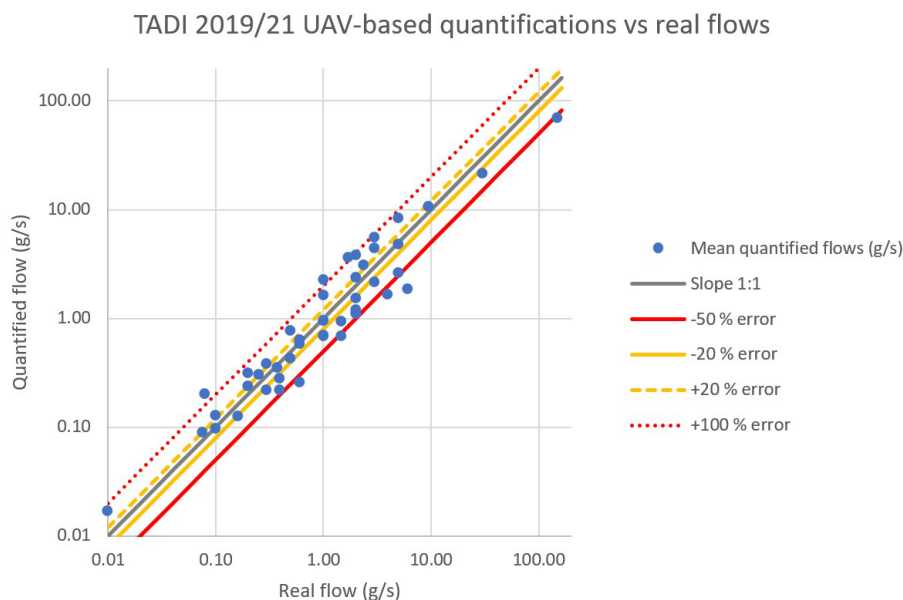

Figure 8. Comparison of emissions quantifications as a function of the real CH_4 emissions fluxes (in $g\,s^{-1}$), as blue dots. A log–log scale is used. The plain-grey line indicates the 1/1 slope or 0 % error. Plain and dashed yellow lines respectively indicate the -20 % and $+20$ % relative error limits. Plain and dotted red lines respectively indicate the -50 % and $+100$ % error limits.

3.3.3 Sources of uncertainties of our emissions quantification approach

This mass balance approach could integrate a direct computation of uncertainties based on the propagation of measurements uncertainties from the wind and from the concentra-tions, but these calculations were not integrated into the currently developed algorithm. This will be the subject of further developments. However, the uncertainties of the mass balance approach are not limited to the instrumental uncertainties. Other sources of uncertainties are associated (i) with

Table 3. Statistics of the relative errors of quantifications during the TADI campaigns, for the release experiments quantified by 1, 2, 3 or 4 independent flights and for the total of all quantifications.

Quantification relative errors (%)					Number of experiments
Median	Average	σ	Minimum	Maximum	
With one quantification flight					
−28	−8	53	−58	125	19
With two quantifications flights					
12	17	57	−69	149	19
With three quantifications flights					
27	23	49	−32	70	4
With four quantifications flights					
19	21	4	19	26	3
All quantifications					
−5	7	53	−69	149	45

the vertical interpolation between the successive horizontal transects where concentration measurements are performed, as information is missing between these levels (ii) and with the turbulent nature of atmospheric transport and the fact that the measurements do not represent either an instantaneous picture nor an average situation of the plume (the monitoring of the concentrations with the UAV is performed along a trajectory within several minutes during which the plume changes, and the wind profile is measured at a low frequency and at a non-neglectable distance from the UAV flight plan). These sources of uncertainties are more difficult to estimate than the propagation of instrumental uncertainties. The wind variability can be estimated based on measurements, but the effect of the vertical interpolation is more difficult to estimate. The orders of magnitudes of uncertainties associated with the concentration and with the wind are analyzed hereafter.

In-flight performances of the AUSEA instruments may be different from the performances achieved during the laboratory experiments under controlled temperature and pressure conditions without any mechanical perturbations due to the vibrations of the UAV. The in-flight accuracies of our measurements cannot be estimated from these experiments as there was no reference instrument. We evaluate the precision of the concentration measurements for each flight as the median value of the 1 s rolling standard deviation (median value is being used to avoid the influence of the real measured spikes within the plumes). These values are given in Tables S1 and S2 for CH_4 and CO_2. The precision of the CH_4 concentration measurements for all flights is always below ± 0.3 ppm. The median value of the in-flight CH_4 precision at 1 s was 118 ppb in 2019 and 30 ppb in 2021. This important

difference in the precision of the CH_4 measurements depicts strong improvements of the 395 analyzers between the 2019 and the 2021 campaigns. For CO_2, values of each flight are not shown in Tables S1 and S2, but the median value of the in-flight CO_2 precision at 1 s reaches 0.3 ppm in 2019 and 0.2 ppm in 2021.

Uncertainties linked with the concentration may result both from the instrumental precision and from the amplitude of the signal (signal-to-noise ratio). We calculated the signal-to-noise ratio considering the signal as the amplitude of the measured concentrations and the noise as the median value of the 1 s rolling standard deviation. Compared to the signal level on the order of magnitude of 10 to 10^2 ppm for CH_4 and the measurement uncertainties on the order of magnitude of 10^{-1} to 10^{-2} ppm, the signal-to-noise ratios of each flight, presented on Tables S1 and S2, are always good, ranging from 38 to 8017, with a median value of 618. As presented in Fig. S1 in the Supplement, our result show that the envelop of the distribution of quantification errors follows a decreasing trend, with increasing signal-to-noise ratios. The highest quantification errors of 182 % correspond to a signal-to-noise ratio of 132, while the flight with the highest signal-to-noise value of 8017 reaches quantification error of 25 %. This would indicate that the signal-to-noise ratio is an indicator of the quality of the quantification.

One could expect the signal-to-noise ratio to be determined by the flow of emitted CH_4 and thus have a link between the performances of the quantification and the emitted flow: Table 4 presents a classification of the quantifications in terms of performance classes for different ranges of real CH_4 emission fluxes. However, the performances of our quantifications do not show any trend dependent on the emissions (Table 4). In fact, the signal-to-noise ratio is not related to the emitted flow, as the distance of the flight plan and the source can be different for each flight.

A comparable study using mass balance emissions quantification with UAV-based measurements (Andersen et al., 2021) noticed that the wind was the dominant source of uncertainty and that the final uncertainty of the quantification could be assimilated with the wind variability. In our case, the instrumental precisions for the wind speed and direction measurements by the lidar are only ± 0.1 m s^{-1} and $\pm 0.5°$. Another source of uncertainty for the wind measurement is associated with the vertical interpolation of the wind profiles between successive measurement levels, but this error cannot be estimated. It has been shown in the literature (Yang et al., 2018; Morales et al., 2022) that low and unstable wind conditions could bring higher quantification errors for comparable mass balance method based on UAV measurements: a threshold of 2.3 m s^{-1} for minimum wind speed and 33.1° for maximum standard deviation of wind direction is considered the limit for good wind conditions. We present the mean and standard deviation of the wind speed and the standard deviation of the wind direction at 1.5 m for each flight of the TADI campaigns in Tables S1 and S2. It can be noted

Table 4. Statistics of the quantifications results for different categories of real emitted fluxes: between 0.01 and 0.3 g s^{-1}, between 0.3 and 1 g s^{-1}, between 1 and 2 g s^{-1}, between 2 and 5 g s^{-1}, and between 5 and 151 g s^{-1} and for the whole range between 0.01 and 151 g s^{-1}. The average relative error is given (in %) for each category, as well as the number of controlled-release experiments for which the quantifications reached relative error categories between -20% and $+20\%$, between -50% and $+100\%$, and between -69% and $+150\%$. Bold numbers correspond to the total number of controlled-release experiments within each real emitted flux category.

			Real emitted flux categories (g s^{-1})					
			[0.01–0.3[	[0.3–1[	[1–2[	[2–5[	[5–151[	[0.01–151]
		Average relative error (%)	38	−10	15	7	−18	
Relative error categories	[−20 % : +20 %[	Number of experiments	3	3	2	1	2	11
	[−50 % : +100 %[		8	8	6	9	5	36
	[−69 % : +150 %[		**9**	**10**	**9**	**10**	**7**	**45**

that these variabilities are of several orders of magnitudes above the instrumental uncertainties of the wind measurements (± 0.1 m s^{-1} and $\pm 0.5°$). In our case, only 26 flights would be considered under good wind conditions while 54 flights were performed under such bad wind conditions (see Tables S1 and S2). Contrary to what was expected, no link has been noticed between the mean or standard deviation of the wind speed or the standard deviation of the wind direction and the relative errors of the quantifications (Figs. S2–S4 in the Supplement).

One would logically expect an improvement of precision when averaging the results of multiple quantification flights for the same source, as this would approximate a mean plume distribution and lower the effect of the turbulent nature of the wind, considering a constant source and wind. However, no significant difference can be observed between quantifications of controlled-release experiments based on one, two, three, or four flights (Tables 3 and 4): the dispersion of results is slightly lower for the quantifications based on four flights (minimum and maximum relative error of 19 % and 26 % only), but this result cannot be considered statistically valid since it concerns only three controlled-release experiments.

3.3.4 Discussion

Experiments conducted during the TADI campaigns allowed our emissions quantification method to be validated, which depicted similar performances for CH$_4$ emissions on a wide spectrum of fluxes, the orders of magnitude ranging between 10^{-2} and 10^{+2} g s^{-1}. The detection limit is most probably determined by the signal-to-noise ratio of the concentration measurements. As the flight plan distance to the source can be adapted for each flight to increase or decrease the level of signal (either to measure signal out the noise level, or to avoid saturation), absolute lower and upper detection limits depend on the conditions on the field (potential flight restrictions affecting the horizontal or vertical area covered by measurements, particular wind conditions, etc.).

If the validation of our method has been done specifically for CH$_4$ emissions quantification, it can easily be extrapolated to the quantification of CO$_2$ emissions, as long as the signal-to-noise ratio is sufficient (this can be controlled for each flight).

No clear link has been found between the quantification error and parameters like the mean and stability of the wind or the flow of emissions. One can suppose that the quantification error is determined either by multiple parameters simultaneously or by other parameters, among which some are difficult to quantify (e.g., distance of the transects to the source, angle between transects and wind direction, length of the transects, vertical gap between transects, oversampling or undersampling of the plume between different horizontal transects, missing top or bottom of the plume). One could expect uncertainties associated with the vertical interpolation to decrease while increasing the number of horizontal transects measured. This could be the subject of future experiments and analyses.

Analyzing the sources of uncertainties in our quantification method, it is clear that a large source of uncertainties is linked to the knowledge of the wind speed and direction. Wind profile measurements were performed with a lidar during the TADI campaigns. As the emission sources were at low elevation from the ground and as the measurements were performed at a relatively short distance, thus with low vertical mixing, most flights were performed at low elevations, in particular in 2019 (typically below 12 m a.g.l.). In such conditions, wind profile measurements could have been performed with alternative devices such as multiple ultrasonic wind sensors sprayed along a vertical mast of a few meters, instead of a lidar which is unable to measure between the meteorological station at 1.5 m.a.g.l. and the first lidar level at 11 m a.g.l. In 2021, the distance between the flight plan and the source was generally longer than in 2019, and some of the flights reached higher altitudes (up to 35 m a.g.l.), thus requiring the use of a lidar. For low elevations (below the first lidar level) the uncertainties associated with wind speed mea-

surements would be expected to be higher than for a within the range of levels monitored by the lidar. The interpolation of the wind speed between 1.5 and 11 m was performed using a simple logarithmic regression, which does not necessarily perfectly match the real vertical wind profile. This brings a larger uncertainty and bias into our quantifications in the case of low plumes, such as those encountered during most of the TADI experiments. We expect better results at higher elevations within the elevation range of the lidar observations. Furthermore, the monitoring frequency of the employed lidar technology was relatively low (15 to 20 s), which does not allow a good representation of the wind variability at the timescale of atmospheric turbulence at low elevation. In addition to the non-negligible distance between the lidar monitoring area and the UAV, this supports the need to develop high-frequency wind monitoring directly on board the UAV. In addition, conditions of low wind speed and variable wind directions were often encountered during the TADI campaigns, which is also challenging for emissions quantification as it is associated with more instabilities of the wind direction and thus an uneasy definition of the measurement plane. Considering these multiple suboptimal conditions, higher precisions could be expected for the monitoring of large and/or high sources such as offshore platforms, stacks or flares which rarely experience low wind conditions.

Our flux estimates from the TADI campaigns can be compared to the performances of other commonly used methods. As described earlier, our quantification method obtained 24 % of results between −20 % and +20 % relative error compared to the true values and 80 % of results between −50 % and +100 %, and all the results were within the range of −69 % to +150 % compared to the true values. Several technologies using UAVs, airplanes or mobile ground measurements were tested and compared during the international Stanford/EDF Mobile Monitoring challenge (Ravikumar et al., 2019) at the Methane Emissions Technology Evaluation Center (METEC), in Colorado, United States, and at a facility near Sacramento, California, United States. The performances of our method are better than the those of the other techniques compared within this challenge: only one method (Seek Ops Inc., based on drone observations) had all quantifications between −90 % and 1000 % but with only 36 % of quantifications in the −50 % to +100 % interval, while the best performance on the −50 % to +100 % interval was achieved by Ball Aerospace plane observations with 53 % of quantifications within this range. Emitted fluxes were generally lower for the Stanford/EDF challenge (from 0 to 0.1 g s^{-1} on METEC and 0 to 7 g s^{-1} at Sacramento) than for our TADI intercomparison experiments (from 0.01 to 150 g s^{-1}), but, as stated earlier, our results are similar for a subset of experiments focusing on the lowest emitted fluxes.

Other methods for CO_2 and CH_4 source tracking and emissions quantification include measurements with CRDS analyzers from cars. An evaluation of such a technique coupled with an atmospheric inversion based on a Gaussian plume dispersion model has been carried out under conditions comparable with our study during a TADI intercomparison campaign in 2018 (Kumar et al., 2021). Results of this validation campaign depicted a good accuracy of the emissions quantification, with estimates of the CH_4 and CO_2 release rates with ~ 10 % to 40 % average relative errors. But only a limited number of 16 out of 50 controlled releases could be monitored, as this technique is constrained by the ability to drive through the plume, which is not possible for high-elevation plumes (in cases of high stacks or plume rise) or for wind direction incompatible with the road infrastructure.

A UAV-based CH_4 emissions quantification method with a near-field Gaussian plume inversion model (Shah et al., 2020) obtained large uncertainties compared to our method with respective lower and upper uncertainty bounds on average of 17 % ± 10 % (1σ) and 227 % ± 98 % (1σ) of the controlled emission flux. Gaussian approaches rely on hypotheses such as a well-mixed plume (problematic at a short distance from the source), a flat terrain, and uniform and constant wind conditions, which are not necessarily true and may be less detrimental for mass balance approaches. The higher acquisition frequency of our analyzer compared to this study is also a technical advantage which leads to better spatially resolved measurements and therefore an improved representation of the plume.

A recently published UAV-based emission quantification technique also relying on a mass balance approach (Morales et al., 2022) was tested on a short range of release rates (0.26 to 0.48 g s^{-1}) and obtained an average bias of −1 % and RMSE of errors of +69 %. These results are comparable with the average and standard deviation of our residuals (+7 % and +53 %), which supports the validity of the mass balance method for the quantification of greenhouse gas emissions. The main differences compared to our approach were the use of only low-level sonic anemometers to measure wind speed and direction, without real monitoring of the vertical wind profile, and the quantification of CH_4 emissions exclusively with a heavier sensor (2.1 kg compared to 1.4 kg for our sensor).

3.4 Application to offshore oil and gas facility emissions quantification

3.4.1 Protocol of offshore platform monitoring campaigns

A 1 d measurement campaign was conducted in the North Sea on April 2019 to quantify the emissions of two offshore platforms (hereafter named P1 and P2). These platforms are equipped with power generators and gas turbines driving the compressors, both emitting CO_2 to the atmosphere. Stacks of the gas turbine are at 50 m above sea level (m a.s.l.) with vertical ejection, and stacks of the power generator are at 30 m.a.s.l. with horizontal ejection. The main source of CH_4 emissions is the gas venting system, at 80 m

above the sea surface, emitting mainly methane with vertical ejection. Other potential minor sources of CH_4 are expected: fugitive emissions and unburned CH_4 in the turbine smokes.

Measurements were carried out from a supply boat chartered on purpose by the company from Den Helder harbor, the Netherlands (Fig. 9a and b). The deck was used as a take-off and landing site for the UAV. The wind lidar installed on the deck recorded wind profiles at 10 levels between 15 and 300 m a.s.l. (Fig. 9b). Real-time concentration measurements were visualized by a person assisting the pilot to adapt the UAV trajectory to the position of the plumes and manage wind direction fluctuations. The duration of each flight was 10 to 20 min. Each flight can be assigned to a trial in terms of concentration recording and emission calculation. The first flight is often a detection flight aiming at localizing the plume and not always usable for emission quantification. Eight and seven repeated flights and emissions quantifications, respectively, were conducted for the monitoring of both platforms (see Table S3 in the Supplement).

Our UAV-based quantifications of CO_2 and CH_4 emissions are presented as relative differences to reference daily averaged emissions calculated by the operator of the platform. The reference emissions calculations from the platform are based on real measurements on the day of comparison, using mass balance and processing data (venting) and combustion balance (gas turbines and power generator). They are expected to be reliable for CO_2 emissions, as they are based on reliable input data (combustion flows, gas composition, CO_2 conversion of hydrocarbons) but assume the proper functioning of equipment, which can be a source of errors for CH_4 emissions (e.g. unexpected open valves or leaks). They also do not reflect the intermittency of the platform operation.

3.4.2 Offshore platform emissions quantifications

During this campaign, the distances between the source and the measurement plane varied between approximately 150 and 450 m depending on the flight (Table S3). To match the vertical distribution of the plumes, originating from sources at typical elevations around 80 m a.s.l., horizontal transects were performed within the range of 50 to 120 m a.s.l. The signal-to-noise ratios obtained during the flights range from 78 to 4337 for CH_4 and from 66 to 523 for CO_2 (Table S3) and thus comparable for both species to the ratios obtained during the TADI campaign (for CH_4 only).

Figure 10 presents typical wind conditions for one flight (2_P2) of the offshore platforms emissions monitoring campaign. Stable wind directions were observed during this flight (Fig. 10a) with similar wind directions for all horizontal transects. The absence of strong shear in the wind direction during our measurements allowed emission plumes to be captured within a single measurement plane for each flight. The wind speed profile of this example is typical for this offshore campaign (Fig. 10b), with a logarithmic profile below 40 m and increasing wind speeds above this limit, typical for stable

atmospheric conditions. The average and standard deviations of the wind speed and the standard deviation of the wind directions at the elevation of the drone are presented for all flights in Table S3. Similar stable wind conditions were encountered for all flights, with mean wind speeds ranging from 7.4 ± 3.0 to $10.6 \pm 2.9\,\mathrm{m\,s^{-1}}$ and standard deviations of the wind direction below $14.4°$. These wind conditions were better than those encountered during the TADI campaigns.

Results of the emission quantifications of both offshore platforms are presented in Table 5. The quantified emission fluxes are presented in terms of relative difference compared to reference daily-average fluxes estimated for the platforms by mass balance and combustion calculation, thus non-representative of short-time variations of emissions.

For the quantification of CH_4 emissions, 13 flights were used among 15 flights (7 for platform P1 and 6 for platform P2), and the first flight for each platform was a short test flight to find the plume position. The mean CH_4 emission quantification for all seven flights for P1 platform presents a 46 % relative difference compared to the reference vent stack expected emissions. This difference is 12 % for the P2 platform. At the timescale of individual flights, large variations in the CH_4 emissions quantification are observed for both platforms, with estimates varying between +8 % and +128 % for the P1 platform and between −60 % and +229 % for the P2 platform, compared to the daily reference emissions. For the P2 platform, the highest estimate of CH_4 emissions corresponds to a single flight (+229 %) largely above the average and standard deviation values of the other five flights ($-31\,\% \pm 18\,\%$). The vertical profile of CH_4 fluxes by transect levels for this particular flight (not shown) depicts an important flux of CH_4 at an elevation lower than the usual main plume observed for all other flights. It is therefore reasonable to interpret this flux value as a short-term event of emissions from a different source than those used for the reference daily average estimates.

The mean values of the methane emissions quantification for all flights combined are comparable although higher than reference daily averaged emissions (+46 % and +12 % for P1 and P2). Our quantification method should be representative of the actual emissions of the whole platform, including fugitive emissions. Reference fluxes are based on estimation using emission factors, gas composition and flow rate measurements or estimation. The higher methane emissions of platform P1 from our method compared to the reference emissions led to a review of some of the platform processes during which an unexpected emission was detected and repaired from a defect valve. A significant emission reduction is expected after the repair. Repeated measurements would be helpful to confirm the actual improvement.

Concerning the quantification of CO_2 emissions, seven flights could be used for emissions quantification for platform P1, while only four flights are used for platform P2, as the CO_2 plume was not entirely captured by our flight plans during some flights, contrary to the CH_4 plume, as dif-
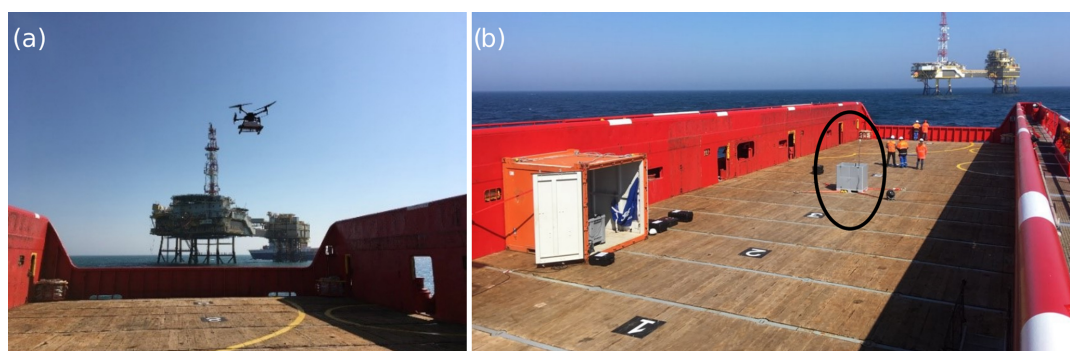
Figure 9. Picture of operations nearby offshore platforms in the North Sea on 19 April 2019, showing **(a)** the UAV equipped with the AUSEA sensor and **(b)** the deck of the supply vessel serving as the take-off and landing site for the UAV, with the wind lidar (black circle).
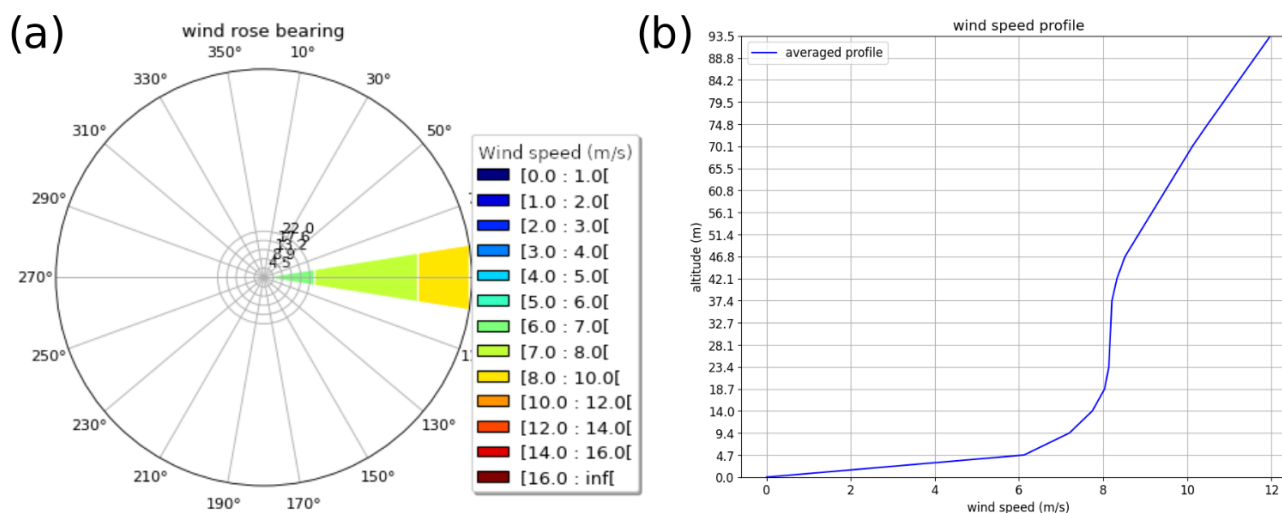

Figure 10. Typical weather conditions for flight 2_P2 of the offshore platform monitoring campaign: **(a)** distributions of wind directions (percentage, with 20° resolution) for different wind speeds classes (color scale, in m s^{-1}) during flight measured by the lidar at the lowest level. **(b)** Averaged wind speed (m s^{-1}) vertical profile (in m a.s.l.) over the flight duration, measured by wind lidar at each of its monitoring level.

ferent sources are involved for both species. The CO$_2$ emissions quantifications are expressed as a relative difference to the daily averaged reference emissions. The estimated CO$_2$ emissions relative difference to the reference emissions are on average for all flights −21 % for platform P1 and −47 % for platform P2. Emissions quantifications of each independent flight provided variable results, with minimal and maximal values of −39 % to +14 % for platform P1 and between −28 % and +2 % for platform P2, thus within the precision of our quantification method. Part of the temporal variability of the CO$_2$ emissions quantification of platform P1 could also be explained by the presence of a supply vessel which arrived and left the platform during the two flights with the highest emissions quantified. Part of the quantified CO$_2$ emissions of both flights could therefore be attributed to the emissions of this supply vessel. If only the other five flights are considered, the averaged quantification of CO$_2$ emissions would be −31 % ± 18 % relative difference compared to the

reference value for platform P1, with a maximum value of −20 %.

Altogether, our emissions quantifications depict large variations between the different flights, for CO$_2$ and more particularly for CH$_4$ fluxes (Table 5). Such variations can be linked with real short-term variations of the emissions over the monitoring period, which are not reflected by the reference emissions values provided at a daily resolution only.

For some flights of this campaign, the measurements did not properly cover the entire plume cross-section vertically (values of $q(z)$ did not reach zero). Therefore, the plume vertical boundaries were estimated from Gaussian interpolations of the vertical distribution of $q(z)$. Better flight plans including measurements below and above the plumes would be necessary for improved quantifications and will be an important requirement of future monitoring protocols.

Table 5. Statistics of the distribution of quantified emissions for all seven flights associated with each platform P1 and P2, for CO_2 and CH_4, expressed as relative differences (in %) to the reference daily average emission rates obtained by mass balance and combustion efficiency calculations.

Species	Relative errors to site calculations (%)			
	CO_2		CH_4	
Platform (number of flights)	P1 (seven flights)	P2 (four flights)	P1 (seven flights)	P2 (six flights)
Minimum	−39	−28	8	−60
First quartile	−36	−26	28	−33
Median	−23	−19	32	−21
Third quartile	−12	−9	51	−17
Maximum	14	2	128	229
Mean	−21	−16	46	12

4 Conclusions

This study presents a complete measurement system for the quantification of atmospheric emissions based on a new atmospheric CO_2 and CH_4 concentration analyzer embarked under a UAV associated with a mass balance box model.

In-lab validation of the analyzer allowed its precision to be estimated (10 ppb for CH_4 and 1 ppm for CO_2 when 615 averaged at 1 Hz) and excellent linearity to be depicted compared to a reference instrument, with good accuracy and repeatability (below 3 % for CH_4 and 1 % for CO_2). In-flight instrumental precision was evaluated to be 118 ppb in 2019 and 30 ppb in 2021 for CH_4 (depicting improvements of the analyzer) and 0.3 ppm for CO_2, whereas for the in-flight accuracy, no intercomparison with a reference instrument was performed in-flight, which could be the subject of future work.

The controlled-release campaigns on the TADI platform in 2019 and 2021 validated the complete emissions quantification method independently of the type of source or carrier and showed better accuracy compared to other current top-of-the-art CO_2 and/or CH_4 emissions quantification techniques using either multispectral cameras, ground-based CRDSs (fixed stations or mobile measurement in a car), wind and gas lidar, infrared camera including concentrations and emissions quantification system, or tunable diode lidar (Ravikumar et al., 2019; Shah et al., 2020; Kumar et al., 2021; Druart et al., 2021) and comparable performances for a similar technique also relying on UAV laser-based concentration monitoring associated with a mass balance model (Morales et al., 2022). This measurement system was already applied on the field and extended in 2022 to more than 100 oil and gas facilities, offshore and onshore, from tropical to high-latitude environments, which will be the subject of upcoming publications. It has a wide range of potential applications, for the quantification of CO_2 or CH_4 sources of diverse anthropogenic or natural origins, such as biogas plants and landfills.

Field applications of our measurement system to offshore oil and gas platforms revealed several assets compared to similar quantification campaigns previously conducted from aircraft or boats. Compared to aircraft-based monitoring, UAVs have the advantage to fly below 300 m high and close to the facilities (distance around 250 m from offshore platforms), allowing the monitoring of the entire plume and the identification of the main sources. The real-time monitoring of the concentration on the ground, associated with the high speed and reactivity of the UAV, provides the possibility for the pilots to adapt the trajectory and fly within the plume despite its meandering. The UAV high speed also allows monitoring of an entire plume within a few minutes, thus representative of a quasi-stationary state, preventing for example double measurements of the same plume when it is meandering, which could occur with measurements conducted from a low-speed vessel. The high frequency of observations (conducted at 24 Hz for these campaigns) allows us to apply a mass balance quantification method which does not require a 2D interpolation (e.g. Kriging) of the measured concentration data but only an interpolation along the vertical direction.

Nevertheless, our measurement system would benefit from further improvements, among which are improved performances of the instrument, of the monitoring protocol or of the modeling.

The simple mass balance method presented here proved able to provide emissions quantifications at low computing costs. Uncertainties were only empirically determined in this study. The quantification method needs further development to propagate the different sources of uncertainties and provide an uncertainty of the emissions quantification. Other modeling approaches could be used: this mass balance method requires concentration measurements throughout an entire plume cross-section, which is not always possible to perform on the field, due to restrictions of the UAV area of operations caused by obstacles or prohibited flight zones. An inverse atmospheric modeling approach with at-

mospheric dispersion models will also be tested in the future (e.g. Darynova et al., 2023). Further experiments and analyses are also required to determine the limits of this method related to the wind stability and minimal wind speed.

A more precise recording of the horizontal and vertical UAV positioning has already been introduced with the use of RTK GPS positioning, facilitating data post-treatment. Future technical development of our method will include wind speed measurements directly on board the UAV, replacing the lidar wind profile measurements for an easier and more cost-effective field deployment. This should also improve the wind speed measurements at elevations below the lowest level of wind lidar measurements (typically below 10 m a.g.l.). A fully automatized UAV operation is also being developed, with UAV track adapting to the plume position, aiming at regular quantifications of O&G facilities.

Future improvements will be made to our greenhouse gas sensor. CO concentration measurements are being developed for future versions of our instrument, which will allow the calculation of a complete combustion efficiency balance for various types of sources of the O&G sector, such as flares. Further weight reduction and adaptations of the instrument will allow it to be embarked by a larger spectrum of air carriers, including VTOL (vertical take-off and landing) UAVs, which have a longer autonomy and fly and higher speed. This will open new applications to monitor emissions of larger-scale sources such as larger industrial facilities, natural sources or small cities.

Author contributions. The manuscript writing was initiated by JLB; completed by NG, LD and LJ; and corrected by all co-authors. The AUSEA sensors and associated spectrometric inversion algorithms were developed at the GSMA by LJ, JC, TD, JB, NC, ND, GA and FPa. In-lab validation of the AUSEA sensor was performed by JLB and DC. Mass balance emission quantification programming and computation of emissions quantifications were conducted by LD and NG. Field monitoring campaigns were conducted by AM, OV, LD and FPi. The project was initiated and coordinated by LJ, LD, OD, CJ and MFB.

References

Allen, G., Hollingsworth, P., Kabbabe, K., Pitt, J. R., Mead, M. I., Illingworth, S., Roberts, G., Bourn, M., Shallcross, D. E., and Percival, C. J.: The development and trial of an unmanned aerial system for the measurement of methane flux from landfill and greenhouse gas emission hotspots, Waste Manage., 87, 883–892, https://doi.org/10.1016/j.wasman.2017.12.024, 2019.

Alvarez, R. A., Zavala-Araiza, D., Lyon, D. R., Allen, D. T., Barkley, Z. R., Brandt, A. R., Davis, K. J., Herndon, S. C., Jacob, D. J., Karion, A., Kort, E. A., Lamb, B. K., Lauvaux, T., Maasakkers, J. D., Marchese, A. J., Omara, M., Pacala, S. W., Peischl, J., Robinson, A. L., Shepson, P. B., Sweeney, C., Townsend-Small, A., Wofsy, S. C., and Hamburg, S. P.: Assessment of methane emissions from the U. S. oil and gas supply chain, Science, 361, 186–188, https://doi.org/10.1126/science.aar7204, 2018.

Andersen, T., Vinkovic, K., de Vries, M., Kers, B., Necki, J., Swolkien, J., Roiger, A., Peters, W., and Chen, H.: Quantifying methane emissions from coal mining ventilation shafts using an unmanned aerial vehicle (UAV)-based active AirCore system, Atmos. Environ. X, 12, 100135, https://doi.org/10.1016/j.aeaoa.2021.100135, 2021.

Ars, S., Broquet, G., Yver Kwok, C., Roustan, Y., Wu, L., Arzoumanian, E., and Bousquet, P.: Statistical atmospheric inversion of local gas emissions by coupling the tracer release technique and local-scale transport modelling: a test case with controlled methane emissions, Atmos. Meas. Tech., 10, 5017–5037, https://doi.org/10.5194/amt-10-5017-2017, 2017.

Berman, E. S. F., Fladeland, M., Liem, J., Kolyer, R., and Gupta, M.: Greenhouse gas analyzer for measurements of carbon dioxide, methane, and water vapor aboard an unmanned aerial vehicle, Sensor Actuat. B-Chem., 169, 128–135, https://doi.org/10.1016/j.snb.2012.04.036, 2012.

Brantley, H. L., Thoma, E. D., Squier, W. C., Guven, B. B., and Lyon, D.: Assessment of Methane Emissions from Oil and Gas Production Pads using Mobile Measurements, Environ. Sci. Technol., 48, 14508–14515, https://doi.org/10.1021/es503070q, 2014.

Brereton, C. A., Joynes, I. M., Campbell, L. J., and Johnson, M. R.: Fugitive emission source characterization using a gradient-based optimization scheme and scalar transport adjoint, Atmos. Environ., 181, 106–116, https://doi.org/10.1016/j.atmosenv.2018.02.014, 2018.

Chen, H., Winderlich, J., Gerbig, C., Hoefer, A., Rella, C. W., Crosson, E. R., Van Pelt, A. D., Steinbach, J., Kolle, O., Beck, V., Daube, B. C., Gottlieb, E. W., Chow, V. Y., Santoni, G. W., and Wofsy, S. C.: High-accuracy continuous airborne measurements of greenhouse gases (CO$_2$ and CH$_4$) using the cavity ring-down spectroscopy (CRDS) technique, Atmos. Meas. Tech., 3, 375–386, https://doi.org/10.5194/amt-3-375-2010, 2010.

Conley, S., Franco, G., Faloona, I., Blake, D. R., Peischl, J., and Ryerson, T. B.: Methane emissions from the 2015 Aliso Canyon blowout in Los Angeles, CA, Science, 351, 1317–1320, https://doi.org/10.1126/science.aaf2348, 2016.

Conley, S., Faloona, I., Mehrotra, S., Suard, M., Lenschow, D. H., Sweeney, C., Herndon, S., Schwietzke, S., Pétron, G., Pifer, J., Kort, E. A., and Schnell, R.: Application of Gauss's theorem to quantify localized surface emissions from airborne measurements of wind and trace gases, Atmos. Meas. Tech., 10, 3345–3358, https://doi.org/10.5194/amt-10-3345-2017, 2017.

Crosson, E. R.: A cavity ring-down analyzer for measuring atmospheric levels of methane, carbon dioxide, and water vapor, Appl. Phys. B, 92, 403–408, https://doi.org/10.1007/s00340-008-3135-y, 2008.

Darynova, Z., Blanco, B., Juery, C., Donnat, L., and Duclaux, O.: Data assimilation method for quantifying controlled methane releases using a drone and ground-sensors, Atmos. Environ. X, 17, 100210, https://doi.org/10.1016/j.aeaoa.2023.100210, 2023.

Druart, G., Foucher, P.-Y., Doz, S., Watremez, X., Jourdan, S., Vanneau, E., and Pinot, H.: Test of SIMAGAZ: a LWIR cryogenic multispectral infrared camera for methane gas leak detection and quantification, in: Algorithms, Technologies, and Applications for Multispectral and Hyperspectral Imaging XXVII, SPIE, 11727, 53–59, https://doi.org/10.1117/12.2586933, 2021.

Dullo, F. T., Lindecrantz, S., Jágerská, J., Hansen, J. H., Engqvist, M., Solbø, S. A., and Hellesø, O. G.: Sensitive on-chip methane detection with a cryptophane-A cladded Mach-Zehnder interferometer, Opt. Express, 23, 31564–31573, https://doi.org/10.1364/OE.23.031564, 2015.

Durry, G. and Megie, G.: Atmospheric CH$_4$ and H$_2$O monitoring with near-infrared InGaAs laser diodes by the SDLA, a balloonborne spectrometer for tropospheric and stratospheric in situ measurements, Appl. Optics, 38, 7342–7354, https://doi.org/10.1364/AO.38.007342, 1999.

Etminan, M., Myhre, G., Highwood, E. J., and Shine, K. P.: Radiative forcing of carbon dioxide, methane, and nitrous oxide: A significant revision of the methane radiative forcing, Geophys. Res. Lett., 43, 12614–12623, https://doi.org/10.1002/2016GL071930, 2016.

Feitz, A., Schroder, I., Phillips, F., Coates, T., Negandhi, K., Day, S., Luhar, A., Bhatia, S., Edwards, G., Hrabar, S., Hernandez, E., Wood, B., Naylor, T., Kennedy, M., Hamilton, M., Hatch, M., Malos, J., Kochanek, M., Reid, P., Wilson, J., Deutscher, N., Zegelin, S., Vincent, R., White, S., Ong, C., George, S., Maas, P., Towner, S., Wokker, N., and Griffith, D.: The Ginninderra CH$_4$ and CO$_2$ release experiment: An evaluation of gas detection and quantification techniques, Int. J. Greenh. Gas Con., 70, 202–224, https://doi.org/10.1016/j.ijggc.2017.11.018, 2018.

Fiehn, A., Kostinek, J., Eckl, M., Klausner, T., Gałkowski, M., Chen, J., Gerbig, C., Röckmann, T., Maazallahi, H., Schmidt, M., Korbeń, P., Neçki, J., Jagoda, P., Wildmann, N., Mallaun, C., Bun, R., Nickl, A.-L., Jöckel, P., Fix, A., and Roiger, A.: Estimating CH$_4$, CO$_2$ and CO emissions from coal mining and industrial activities in the Upper Silesian Coal Basin using an aircraft-based mass balance approach, Atmos. Chem. Phys., 20, 12675–12695, https://doi.org/10.5194/acp-20-12675-2020, 2020.

Forster, P., Storelvmo, T., Armour, K., Collins, W., Dufresne, J.-L., Frame, D., Lunt, D., Mauritsen, T., Palmer, M., and Watanabe, M.: The Earth's energy budget, climate feedbacks, and climate sensitivity, in: Climate Change 2021: The Physical Science Basis. Contribution of Working Group I to the Sixth Assessment Report of the Intergovernmental Panel on Climate Change, Cambridge University Press, Oxford, UK, 923–1054, ISBN 978-92-9169-158-6, 2021.

France, J. L., Bateson, P., Dominutti, P., Allen, G., Andrews, S., Bauguitte, S., Coleman, M., Lachlan-Cope, T., Fisher, R. E., Huang, L., Jones, A. E., Lee, J., Lowry, D., Pitt, J., Purvis, R., Pyle, J., Shaw, J., Warwick, N., Weiss, A., Wilde, S., Witherstone, J., and Young, S.: Facility level measurement of offshore oil and gas installations from a medium-sized airborne platform: method development for quantification and source identification of methane emissions, Atmos. Meas. Tech., 14, 71–88, https://doi.org/10.5194/amt-14-71-2021, 2021.

Golston, L. M., Tao, L., Brosy, C., Schäfer, K., Wolf, B., McSpiritt, J., Buchholz, B., Caulton, D. R., Pan, D., Zondlo, M. A., Yoel, D., Kunstmann, H., and McGregor, M.: Lightweight mid-infrared methane sensor for unmanned aerial systems, Appl. Phys. B, 123, 170, https://doi.org/10.1007/s00340-017-6735-6, 2017.

Golston, L. M., Aubut, N. F., Frish, M. B., Yang, S., Talbot, R. W., Gretencord, C., McSpiritt, J., and Zondlo, M. A.: Natural Gas Fugitive Leak Detection Using an Unmanned Aerial Vehicle: Localization and Quantification of Emission Rate, Atmosphere-Basel, 9, 333, https://doi.org/10.3390/atmos9090333, 2018.

Gorchov Negron, A. M., Kort, E. A., Conley, S. A., and Smith, M. L.: Airborne Assessment of Methane Emissions from Offshore Platforms in the U. S. Gulf of Mexico, Environ. Sci. Technol., 54, 5112–5120, https://doi.org/10.1021/acs.est.0c00179, 2020.

Hirst, B., Jonathan, P., González del Cueto, F., Randell, D., and Kosut, O.: Locating and quantifying gas emission sources using remotely obtained concentration data, Atmos. Environ., 74, 141–158, https://doi.org/10.1016/j.atmosenv.2013.03.044, 2013.

Hmiel, B., Petrenko, V. V., Dyonisius, M. N., Buizert, C., Smith, A. M., Place, P. F., Harth, C., Beaudette, R., Hua, Q., Yang, B., Vimont, I., Michel, S. E., Severinghaus, J. P., Etheridge, D., Bromley, T., Schmitt, J., Faïn, X., Weiss, R. F., and Dlugokencky, E.: Preindustrial $^{14}CH_4$ indicates greater anthropogenic fossil CH_4 emissions, Nature, 578, 409–412, https://doi.org/10.1038/s41586-020-1991-8, 2020.

Huang, Z., Wang, Y., Yu, Q., Ma, W., Zhang, Y., and Chen, L.: Source area identification with observation from limited monitor sites for air pollution episodes in industrial parks, Atmos. Environ., 122, 1–9, https://doi.org/10.1016/j.atmosenv.2015.08.048, 2015.

ICOS RI: ICOS Atmosphere Station Specifications V2.0, edited by: Laurent, O., ICOS ERIC, https://doi.org/10.18160/GK28-2188, 2020.

Jackson, R. B., Down, A., Phillips, N. G., Ackley, R. C., Cook, C. W., Plata, D. L., and Zhao, K.: Natural Gas Pipeline Leaks Across Washington, DC, Environ. Sci. Technol., 48, 2051–2058, https://doi.org/10.1021/es404474x, 2014.

Joly, L., Maamary, R., Decarpenterie, T., Cousin, J., Dumelié, N., Chauvin, N., Legain, D., Tzanos, D., and Durry, G.: Atmospheric Measurements by Ultra-Light SpEctrometer (AMULSE) Dedicated to Vertical Profile in Situ Measurements of Carbon Dioxide (CO_2) Under Weather Balloons: Instrumental Development and Field Application, Sensors, 16, 1609, https://doi.org/10.3390/s16101609, 2016.

Joly, L., Coopmann, O., Guidard, V., Decarpenterie, T., Dumelié, N., Cousin, J., Burgalat, J., Chauvin, N., Albora, G., Maamary, R., Miftah El Khair, Z., Tzanos, D., Barrié, J., Moulin, É., Aressy, P., and Belleudy, A.: The development of the Atmospheric Measurements by Ultra-Light Spectrometer (AMULSE) greenhouse gas profiling system and application for satellite retrieval validation, Atmos. Meas. Tech., 13, 3099–3118, https://doi.org/10.5194/amt-13-3099-2020, 2020.

Karion, A., Sweeney, C., Kort, E. A., Shepson, P. B., Brewer, A., Cambaliza, M., Conley, S. A., Davis, K., Deng, A., Hardesty, M., Herndon, S. C., Lauvaux, T., Lavoie, T., Lyon, D., Newberger, T., Pétron, G., Rella, C., Smith, M., Wolter, S., Yacovitch, T. I., and Tans, P.: Aircraft-Based Estimate of Total Methane Emissions from the Barnett Shale Region, Environ. Sci. Technol., 49, 8124–8131, https://doi.org/10.1021/acs.est.5b00217, 2015.

Khan, A., Schaefer, D., Tao, L., Miller, D. J., Sun, K., Zondlo, M. A., Harrison, W. A., Roscoe, B., and Lary, D. J.: Low Power Greenhouse Gas Sensors for Unmanned Aerial Vehicles, Remote Sens.-Basel, 4, 1355–1368, https://doi.org/10.3390/rs4051355, 2012.

Kumar, P., Broquet, G., Yver-Kwok, C., Laurent, O., Gichuki, S., Caldow, C., Cropley, F., Lauvaux, T., Ramonet, M., Berthe, G., Martin, F., Duclaux, O., Juery, C., Bouchet, C., and Ciais, P.: Mobile atmospheric measurements and local-scale inverse estimation of the location and rates of brief CH_4 and CO_2 releases from point sources, Atmos. Meas. Tech., 14, 5987–6003, https://doi.org/10.5194/amt-14-5987-2021, 2021.

Kumar, P., Broquet, G., Caldow, C., Laurent, O., Gichuki, S., Cropley, F., Yver-Kwok, C., Fontanier, B., Lauvaux, T., Ramonet, M., Shah, A., Berthe, G., Martin, F., Duclaux, O., Juery, C., Bouchet, C., Pitt, J., and Ciais, P.: Near-field atmospheric inversions for the localization and quantification of controlled methane releases using stationary and mobile measurements, Q. J. Roy. Meteor. Soc., 148, 1886–1912, https://doi.org/10.1002/qj.4283, 2022.

Lee, J. D., Mobbs, S. D., Wellpott, A., Allen, G., Bauguitte, S. J.-B., Burton, R. R., Camilli, R., Coe, H., Fisher, R. E., France, J. L., Gallagher, M., Hopkins, J. R., Lanoiselle, M., Lewis, A. C., Lowry, D., Nisbet, E. G., Purvis, R. M., O'Shea, S., Pyle, J. A., and Ryerson, T. B.: Flow rate and source reservoir identification from airborne chemical sampling of the uncontrolled Elgin platform gas release, Atmos. Meas. Tech., 11, 1725–1739, https://doi.org/10.5194/amt-11-1725-2018, 2018.

Liu, S., Yang, X., and Zhou, X.: Development of a low-cost UAV-based system for CH_4 monitoring over oil fields, Environ. Technol., 42, 3154–3163, https://doi.org/10.1080/09593330.2020.1724199, 2020.

Malaver, A., Motta, N., Corke, P., and Gonzalez, F.: Development and Integration of a Solar Powered Unmanned Aerial Vehicle and a Wireless Sensor Network to Monitor Greenhouse Gases, Sensors, 15, 4072–4096, https://doi.org/10.3390/s150204072, 2015.

Masson-Delmotte, V., Zhai, P., Pörtner, H. O., Roberts, D., Skea, J., Shukla, P. R., Pirani, A., Moufouma-Okia, W., Péan, C., and Pidcock, R.: IPCC: Summary for Policymakers, in: Global warming of 1.5 °C. An IPCC Special Report on the impacts of global warming of 1.5 °C above pre-industrial levels and related global greenhouse gas emission pathways, in the context of strengthening the global, Tech. Rep., World Meteorol. Organ., Geneva, https://www.ipcc.ch/sr15/chapter/spm/ (last access: 3 June 2024), 2018.

Mays, K. L., Shepson, P. B., Stirm, B. H., Karion, A., Sweeney, C., and Gurney, K. R.: Aircraft-Based Measurements of the Carbon Footprint of Indianapolis, Environ. Sci. Technol., 43, 7816–7823, https://doi.org/10.1021/es901326b, 2009.

Mønster, J., Kjeldsen, P., and Scheutz, C.: Methodologies for measuring fugitive methane emissions from landfills – A review, Waste Manage., 87, 835–859, https://doi.org/10.1016/j.wasman.2018.12.047, 2019.

Morales, R., Ravelid, J., Vinkovic, K., Korbeń, P., Tuzson, B., Emmenegger, L., Chen, H., Schmidt, M., Humbel, S., and Brunner, D.: Controlled-release experiment to investigate uncertainties in UAV-based emission quantification for methane point sources, Atmos. Meas. Tech., 15, 2177–2198, https://doi.org/10.5194/amt-15-2177-2022, 2022.

Nara, H., Tanimoto, H., Tohjima, Y., Mukai, H., Nojiri, Y., and Machida, T.: Emissions of methane from offshore oil and gas platforms in Southeast Asia, Sci. Rep.-UK, 4, 6503, https://doi.org/10.1038/srep06503, 2014.

Nathan, B. J., Golston, L. M., O'Brien, A. S., Ross, K., Harrison, W. A., Tao, L., Lary, D. J., Johnson, D. R., Covington, A. N., Clark, N. N., and Zondlo, M. A.: Near-Field Characterization of Methane Emission Variability from a Compressor Station Using a Model Aircraft, Environ. Sci. Technol., 49, 7896–7903, https://doi.org/10.1021/acs.est.5b00705, 2015.

Neumann, P. P., Bennetts, V. H., Lilienthal, A. J., Bartholmai, M., and Schiller, J. H.: Gas source localization with a micro-drone using bio-inspired and particle filter-based algorithms, Adv. Robotics, 27, 725–738, https://doi.org/10.1080/01691864.2013.779052, 2013.

NF EN 17628: https://www.boutique.afnor.org/fr-fr/norme/nf-en-17628/emissions-fugitives-et-diffuses-concernant-les-secteurs-industriels-methode/fa194272/325170, last access: 30 November 2022.

Ng, R. T. L., Hassim, M. H., and Hurme, M.: A hybrid approach for estimating fugitive emission rates in process development and design under incomplete knowledge, Process. Saf. Environ., 109, 365–373, https://doi.org/10.1016/j.psep.2017.04.003, 2017.

Oil and Gas Methane Partnership (OGMP) 2.0 Framework: https://www.ccacoalition.org/en/resources/oil-and-gas-methane-partnership-ogmp-20-framework, last access: 4 July 2022.

O'Keefe, A.: Integrated cavity output analysis of ultra-weak absorption, Chem. Phys. Lett., 293, 331–336, https://doi.org/10.1016/S0009-2614(98)00785-4, 1998.

O'Keefe, A., Scherer, J. J., and Paul, J. B.: cw Integrated cavity output spectroscopy, Chem. Phys. Lett., 307, 343–349, https://doi.org/10.1016/S0009-2614(99)00547-3, 1999.

Ravikumar, A. P., Sreedhara, S., Wang, J., Englander, J., Roda-Stuart, D., Bell, C., Zimmerle, D., Lyon, D., Mogstad, I., Ratner, B., and Brandt, A. R.: Single-blind inter-comparison of methane detection technologies – results from the Stanford/EDF Mobile Monitoring Challenge, Elem. Sci. Anthr., 7, 37, https://doi.org/10.1525/elementa.373, 2019.

Riddick, S. N., Mauzerall, D. L., Celia, M., Harris, N. R. P., Allen, G., Pitt, J., Staunton-Sykes, J., Forster, G. L., Kang, M., Lowry, D., Nisbet, E. G., and Manning, A. J.: Methane emissions from oil and gas platforms in the North Sea, Atmos. Chem. Phys., 19, 9787–9796, https://doi.org/10.5194/acp-19-9787-2019, 2019.

Rivera Martinez, R., Santaren, D., Laurent, O., Cropley, F., Mallet, C., Ramonet, M., Caldow, C., Rivier, L., Broquet, G., Bouchet, C., Juery, C., and Ciais, P.: The Potential of Low-Cost Tin-Oxide Sensors Combined with Machine Learning for Estimating Atmospheric CH$_4$ Variations around Background Concentration, Atmosphere-Basel, 12, 107, https://doi.org/10.3390/atmos12010107, 2021.

Romanini, D., Chenevier, M., Kassi, S., Schmidt, M., Valant, C., Ramonet, M., Lopez, J., and Jost, H.-J.: Optical–feedback cavity–enhanced absorption: a compact spectrometer for real–time measurement of atmospheric methane, Appl. Phys. B, 83, 659–667, https://doi.org/10.1007/s00340-006-2177-2, 2006.

Saunois, M., Stavert, A. R., Poulter, B., Bousquet, P., Canadell, J. G., Jackson, R. B., Raymond, P. A., Dlugokencky, E. J., Houweling, S., Patra, P. K., Ciais, P., Arora, V. K., Bastviken, D., Bergamaschi, P., Blake, D. R., Brailsford, G., Bruhwiler, L., Carlson, K. M., Carrol, M., Castaldi, S., Chandra, N., Crevoisier, C., Crill, P. M., Covey, K., Curry, C. L., Etiope, G., Frankenberg, C., Gedney, N., Hegglin, M. I., Höglund-Isaksson, L., Hugelius, G., Ishizawa, M., Ito, A., Janssens-Maenhout, G., Jensen, K. M., Joos, F., Kleinen, T., Krummel, P. B., Langenfelds, R. L., Laruelle, G. G., Liu, L., Machida, T., Maksyutov, S., McDonald, K. C., McNorton, J., Miller, P. A., Melton, J. R., Morino, I., Müller, J., Murguia-Flores, F., Naik, V., Niwa, Y., Noce, S., O'Doherty, S., Parker, R. J., Peng, C., Peng, S., Peters, G. P.,

Prigent, C., Prinn, R., Ramonet, M., Regnier, P., Riley, W. J., Rosentreter, J. A., Segers, A., Simpson, I. J., Shi, H., Smith, S. J., Steele, L. P., Thornton, B. F., Tian, H., Tohjima, Y., Tubiello, F. N., Tsuruta, A., Viovy, N., Voulgarakis, A., Weber, T. S., van Weele, M., van der Werf, G. R., Weiss, R. F., Worthy, D., Wunch, D., Yin, Y., Yoshida, Y., Zhang, W., Zhang, Z., Zhao, Y., Zheng, B., Zhu, Q., Zhu, Q., and Zhuang, Q.: The Global Methane Budget 2000–2017, Earth Syst. Sci. Data, 12, 1561–1623, https://doi.org/10.5194/essd-12-1561-2020, 2020.

Shah, A., Pitt, J. R., Ricketts, H., Leen, J. B., Williams, P. I., Kabbabe, K., Gallagher, M. W., and Allen, G.: Testing the near-field Gaussian plume inversion flux quantification technique using unmanned aerial vehicle sampling, Atmos. Meas. Tech., 13, 1467–1484, https://doi.org/10.5194/amt-13-1467-2020, 2020.

Shindell, D., Kuylenstierna, J. C. I., Vignati, E., van Dingenen, R., Amann, M., Klimont, Z., Anenberg, S. C., Muller, N., Janssens-Maenhout, G., Raes, F., Schwartz, J., Faluvegi, G., Pozzoli, L., Kupiainen, K., Höglund-Isaksson, L., Emberson, L., Streets, D., Ramanathan, V., Hicks, K., Oanh, N. T. K., Milly, G., Williams, M., Demkine, V., and Fowler, D.: Simultaneously Mitigating Near-Term Climate Change and Improving Human Health and Food Security, Science, 335, 183–189, https://doi.org/10.1126/science.1210026, 2012.

Terry, C., Argyle, M., Meyer, S., Sander, L., and Hirst, B.: Mapping methane sources and their emission rates using an aircraft, Lead. Edge, 36, 33–35, https://doi.org/10.1190/tle36010033.1, 2017.

Tuzson, B., Graf, M., Ravelid, J., Scheidegger, P., Kupferschmid, A., Looser, H., Morales, R. P., and Emmenegger, L.: A compact QCL spectrometer for mobile, high-precision methane sensing aboard drones, Atmos. Meas. Tech., 13, 4715–4726, https://doi.org/10.5194/amt-13-4715-2020, 2020.

UNFCCC: Glasgow Climate Pact, https://unfccc.int/documents/310475, last access: 2 December 2021.

Worden, J. R., Bloom, A. A., Pandey, S., Jiang, Z., Worden, H. M., Walker, T. W., Houweling, S., and Röckmann, T.: Reduced biomass burning emissions reconcile conflicting estimates of the post-2006 atmospheric methane budget, Nat. Commun., 8, 2227, https://doi.org/10.1038/s41467-017-02246-0, 2017.

Xia, J., Zhu, F., Zhang, S., Kolomenskii, A., and Schuessler, H.: A ppb level sensitive sensor for atmospheric methane detection, Infrared Phys. Techn., 86, 194–201, https://doi.org/10.1016/j.infrared.2017.09.018, 2017.

Yacovitch, T. I., Daube, C., and Herndon, S. C.: Methane Emissions from Offshore Oil and Gas Platforms in the Gulf of Mexico, Environ. Sci. Technol., 54, 3530–3538, https://doi.org/10.1021/acs.est.9b07148, 2020.

Yang, S., Talbot, R. W., Frish, M. B., Golston, L. M., Aubut, N. F., Zondlo, M. A., Gretencord, C., and McSpiritt, J.: Natural Gas Fugitive Leak Detection Using an Unmanned Aerial Vehicle: Measurement System Description and Mass Balance Approach, Atmosphere-Basel, 9, 383, https://doi.org/10.3390/atmos9100383, 2018.

Yver Kwok, C., Laurent, O., Guemri, A., Philippon, C., Wastine, B., Rella, C. W., Vuillemin, C., Truong, F., Delmotte, M., Kazan, V., Darding, M., Lebègue, B., Kaiser, C., Xueref-Rémy, I., and Ramonet, M.: Comprehensive laboratory and field testing of cavity ring-down spectroscopy analyzers measuring H$_2$O, CO$_2$, CH$_4$ and CO, Atmos. Meas. Tech., 8, 3867–3892, https://doi.org/10.5194/amt-8-3867-2015, 2015.